# Radiative Effects of Cloud-Type Variations

TING CHEN

*Department of Earth and Environmental Sciences, Columbia University, New York, New York*

WILLIAM B. ROSSOW

*NASA/Goddard Institute for Space Studies, New York, New York*

YUANCHONG ZHANG

*Department of Applied Physics and Applied Mathematics, Columbia University, New York, New York*

(Manuscript received 9 November 1998, in final form 16 March 1999)

ABSTRACT

Radiative flux changes induced by the occurrence of different cloud types are investigated using International Satellite Cloud Climatology Project cloud data and a refined radiative transfer model from National Aeronautics and Space Administration/Goddard Institute for Space Studies general circulation model. Cloud types are defined by their top height and optical thickness. Cloud-type variations are shown to be as important as cloud cover in modifying the radiation field of the earth–atmosphere system. Other variables, such as the solar insolation and atmospheric and surface properties, also play significant roles in determining regional cloud radiative effects. The largest ''annual'' mean (approximated by averaging the results of four particular days, one from each season) changes of the global top-of-atmosphere and surface shortwave radiative fluxes are produced by stratocumulus, altostratus, and cirrostratus clouds (i.e., clouds with moderate optical thicknesses). Cirrus, cirrostratus, and deep convective clouds (i.e., the highest-level clouds) cause most of the annual mean changes in the global top-of-atmosphere longwave radiative fluxes; whereas the largest annual mean changes of the global surface longwave radiative fluxes are caused by stratocumulus, cumulus, and altostratus.

## 1. Introduction

Clouds affect the earth's climate by modulating the vertical and horizontal distributions of solar radiative heating, latent heating, and cooling by thermal radiation that drive the atmospheric circulation. Moreover, clouds alter moisture transports by forming precipitation that returns the evaporated water to the surface. The radiative effects of clouds have been studied for a long time, with observations or numerical models of the atmosphere; but most of these earlier studies have focused on the relationship between the earth radiation budget or surface radiation budget and total cloud cover (see references in Fung et al. 1984; Hartmann et al. 1986; Rossow and Lacis 1990), neglecting the effect of variations of other cloud properties (i.e., cloud types) due to the lack of global quantitative information on the properties of different cloud types (Hartmann and Doelling 1991). Undoubtedly, this focus on the total cloud cover is an oversimplification because cloud-type variations (e.g., variations in cloud-top height and water content) may well affect both shortwave and longwave radiative fluxes as much as changes in total cloud cover and because the distribution and frequency of occurrence of different cloud types could change during climate variations providing another climate feedback. Considering the problem in terms of cloud types may also be necessary to establish an accurate quantitative connection between different kinds of atmospheric motions and cloud radiative properties in order to make reliable climate change predictions. For example, recent studies have shown that the ''anvil'' clouds in tropical mesoscale convective complexes produce large vertical heating rate gradients that enhance convective instability, alter upward energy and water transports in the Tropics, and may help sustain these larger systems over more than one diurnal cycle (e.g., Ackerman et al. 1988; Machado and Rossow 1993). Similar relations may intricately link together atmospheric motions, precipitation, and cloud–radiation interactions, which makes the study of clouds so challenging. A detailed and global investigation of the radiative effects of cloud-type variations is now pos-

*Corresponding author address:* Ting Chen, Department of Earth and Environmental Sciences, Columbia University, 2880 Broadway, New York, NY 10025.
E-mail: tchen@giss.nasa.gov

sible using the cloud datasets produced by the International Satellite Cloud Climatology Project (ISCCP; Schiffer and Rossow 1983; Rossow and Schiffer 1991).

Hartmann and colleagues (Ockert-Bell and Hartmann 1992; Hartmann et al. 1992) carried out the most extensive investigation to date by combining monthly mean, top-of-atmosphere (TOA) radiative fluxes obtained from the Earth Radiation Budget Experiment with monthly mean cloud properties determined by ISCCP. They calculated multivariable, linear regressions of the monthly mean values to determine which cloud types explained changes in the radiative fluxes. The present study looks at these relations in a more direct way by calculating the radiative fluxes directly from the ISCCP cloud data, combined with other atmospheric and surface datasets, using a refined version of the radiative transfer model from the National Aeronautics and Space Administration/Goddard Institute for Space Studies (GISS) general circulation model (GCM; Rossow and Lacis 1990; Zhang et al. 1995). The advantage of our approach is that it better separates the effects of the clouds on the radiation field from other atmospheric and surface factors so that more direct estimations of the radiative effects of individual cloud types can be made. Most importantly, our method also allows us to extend this type of study to include the complete effects of cloud-type variations on the partitioning of the TOA (=100 km) radiation budget into its surface and in-atmosphere components in a self-consistent manner (Rossow and Lacis 1990; Rossow and Zhang 1995).

This particular approach to the diagnosis of cloud-induced radiative effects, based on the earlier technique of calculating fluxes from observed physical quantities, was first outlined in Rossow and Lacis (1990) and has been successfully applied in a series of studies to estimate directly the cloud effects on the various components of earth radiation budget and the meridional energy transports by the atmospheric and oceanic general circulations (Zhang et al. 1995; Rossow and Zhang 1995; Zhang and Rossow 1997). The present paper is part of a continuing study of this important subject and focuses on a simple version of the problem of the radiative effects of cloud-type variations. Several effects are not treated in this study (see section 5), particularly the effects of layer overlap or more complex vertical structure. Here we consider each cloud type to be a single-layered cloud, and in a companion paper the uncertainties in the calculated fluxes due to this simplification are assessed. The results of that study show that the TOA and surface flux uncertainties caused by the oversimplified single-layered cloud treatment are small in the longwave and are negligible in the shortwave compared with other sources of uncertainty (Chen et al. 1999, manuscript submitted to *J. Climate;* Zhang et al. 1995). However, the cloud vertical structure is important to the vertical distribution of radiative heating within the atmosphere.

Section 2 gives a short description of the ISCCP datasets and the definitions of the cloud types used in this study. Section 3 briefly describes the radiative transfer model, as well as the input and output quantities. Section 4 compares the radiative effects of individual cloud types in terms of the cloud-induced radiative flux changes from clear conditions (cf. Rossow and Zhang 1995). Section 5 summarizes the main findings and discusses the implications of our results.

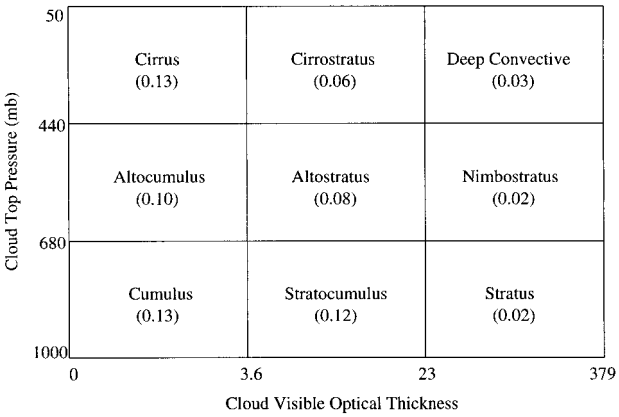


FIG. 1. Definitions of the nine different cloud types used in terms of cloud-top pressure and visible optical thickness. The numbers in the parentheses are the global mean cloud-type amounts from 5 yr (1989–93) of ISCCP D-series data.

## 2. Datasets and cloud-type definitions

ISCCP collects measurements of infrared ($\approx$11 $\mu$m) and visible ($\approx$0.6 $\mu$m) radiances from the imaging radiometers on the operational weather satellites and analyzes them, together with correlative datasets describing the surface and atmosphere, to produce a climatology of cloud properties, including cloud cover fraction, cloud-top pressure/temperature, and cloud optical thickness/water path (Schiffer and Rossow 1985; Rossow and Schiffer 1991). ISCCP D1 data (revised version of the C1 product; Rossow et al. 1996) merges the retrieved quantities from different satellites into a global, 3-hourly product by summarizing the cloud variations at 280-km resolution (equivalent to 2.5° $\times$ 2.5° lat–long at the equator). In addition to the area-averaged cloud parameters within each map grid box, the distribution of cloud parameters is also reported in terms of 15 cloud types, defined by three intervals of cloud-top pressure (high cloud, $P_c \leq 440$ mb; middle cloud, 440 mb $< P_c \leq$ 680 mb; and low cloud, $P_c > 680$ mb), three optical thickness categories ($\tau \leq 3.6$; $3.6 < \tau \leq 23$; and $\tau >$ 23), and the phases of the cloud particles (ice if top temperature <260 K, otherwise liquid). Only mid- and low-level clouds are separated into liquid and ice clouds; all high-level clouds are considered to be ice clouds. Figure 1 illustrates the cloud-type definitions and gives their average global annual mean amounts (for 1989–93). The names used for convenience are meant to sug-

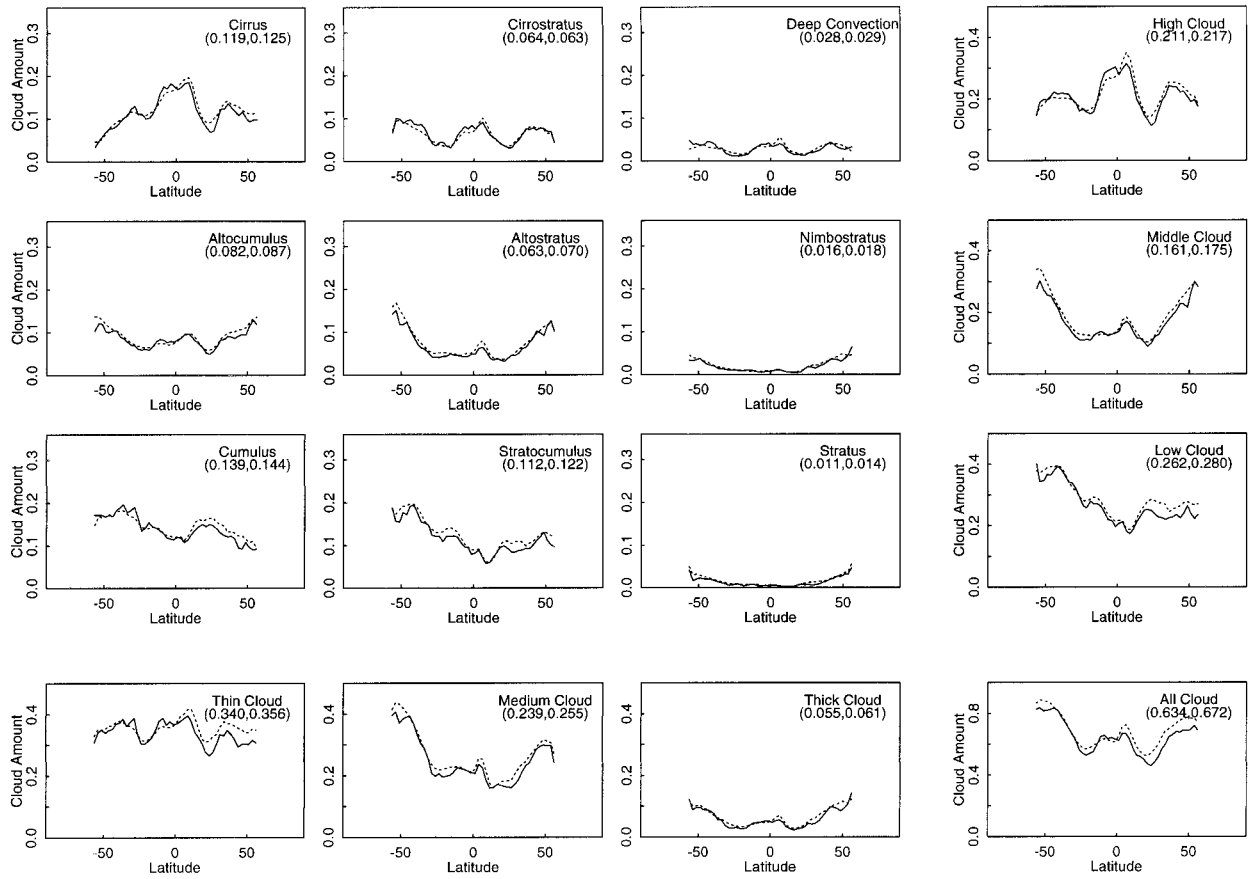


FIG. 2. Zonal mean distributions of cloud amounts averaged over four days (solid line) and averaged over the four corresponding months (dashed line) for the nine different cloud types defined in Fig. 1, for average high, middle, and low clouds, for average optically thin, moderate, and thick clouds, and for the overall average clouds. The first (second) number in the parentheses is the global mean cloud amount value averaged over four days (months).

gest qualitative relationships with the classic morphological cloud types, but they should not be interpreted to be quantitatively correct in every instance (cf. Lau and Crane 1995).

Since cloud optical thicknesses are determined from visible radiance measurements, which are only available during daytime, and the cloud-top temperature is more accurately determined as a function of optical thickness (Rossow et al. 1996), nighttime cloud-type information is refined by interpolating between daytime cloud observations to complete the diurnal cycle. The interpolation procedure involves two steps. 1) The nighttime values of cloud optical thickness and top temperature of individual cloud types are set to be the corresponding values of the ''nearest'' daytime cloud observations (e.g., 2100 is nearer in time to 1800 earlier the same day, but 0300 is nearer to 0600 later the same day). 2) The cloud fractions of individual cloud types during nighttime are adjusted proportionately according to the corresponding daytime proportions of total cloud fraction and the current nighttime total cloud fraction (if no measurement of current nighttime total cloud fraction available, the cloud fraction of each nighttime cloud type is simply set to the corresponding value of the nearest daytime observation). Occasionally, missing daytime observations are filled by replicating the values nearest in time. In the polar regions in some months, there are no daytime cloud observations all month, so we report no results.

The computational resources accessible for this study precluded calculations covering extensive periods of time. As this study is only intended to estimate the relative magnitude of the cloud-type effects, not to determine precise climatological values, we choose to perform calculations on only four days of data. However, since the magnitude of the cloud–radiative effects also depends on the properties of the surface and atmosphere, particularly their seasonal variations as well as the seasonal variation of solar insolation, we choose four specific days from the D1 dataset to provide a representative sample of the large-scale variations of cloud properties, surface and atmospheric temperatures, humidity, and solar zenith angles (one from each season): 15 January, 15 April, 15 July, and 15 October 1991. Figure 2 shows that the zonal mean distributions of all the cloud-type amounts (where we have combined the liquid and ice

forms) averaged over these four days are very similar to the zonal mean distributions averaged over the four whole months. Since the average top pressures and optical thicknesses for each type are constrained by their definitions, they are almost identical for daily and monthly zonal mean values (except for the optical thicknesses of the thickest cloud types, but their radiative effects are already saturated and any small changes in the optical thickness values are less significant radiatively). Comparing individual days and months, the rms differences in zonal mean cloud-type amounts are $<0.02$, in zonal mean cloud-type optical thickness are within 15% of the corresponding values, in zonal mean cloud-type top temperature are $<1$ K for mid- and low-level clouds and $<4$ K for high clouds. The comparison implies that the 4-day averaged values of cloud-type amounts and radiative properties are not qualitatively different from the corresponding 4-month averaged values, so the radiative fluxes computed from the two datasets will be similar to each other. We show in the appendix that using preaveraged input quantities would introduce significant biases (cf. Zhang et al. 1995; Rossow and Zhang 1995).

## 3. Radiative model description

This study uses the same radiative transfer model as described by Zhang et al. (1995) with similar input and output quantities, except as described below.

To simplify the radiative calculations somewhat, we treat all clouds as liquid water clouds by averaging $T_c$, and $\tau$ of the ice/liquid clouds (''radiatively weighted'') according to cloud amounts, reducing the maximum number of cloud types to nine. Hartmann et al. (1992) have shown that the variations in TOA radiative fluxes can be accounted for by the changes of five distinct cloud types; however, as we will show that different cloud types are more important to the surface and in-atmosphere fluxes, we retain all nine types. Since the ISCCP D1 data has retrieved the properties of the colder clouds using an ice microphysical model, this treatment will bias our results somewhat. Mishchenko et al. (1996) show that an ice cloud with the same optical thickness has a $\sim$10% (relative) larger albedo than a liquid water cloud; but these biases are reduced when larger, elongated particles are considered. Nevertheless, our treatment will underestimate cloud albedos and overestimate cloud shortwave transmission for higher-level clouds and at higher latitudes relative to lower-level clouds and lower latitudes. Since we are also underestimating the average particle size for such clouds, the shortwave absorption is also underestimated by less than 1 W m$^{-2}$ on average. The retrieved cloud-top location for optically thin ice clouds is more accurate in the ISCCP D1 data (cf. Minnis et al. 1993; Stubenrauch et al. 1998a); hence the error in longwave fluxes associated with cloud-top location from ISCCP C1 data is smaller by about 1–2 W m$^{-2}$. We have repeated the calculations for one day using a revised radiative transfer model that includes a test version of an ice cloud model; there is no qualitative change in the results reported below (the zonal mean changes in all flux components are smaller than 1 W m$^{-2}$).

The main change to the input parameters is to insert cloud properties for each separate cloud type present in each map grid box; the total fluxes are then the sum of these values weighted by the fractional cover of each cloud type. Zhang et al. (1995) used the area-averaged cloud properties to define a single cloud layer covering a portion of the map grid box. Thus, they calculate up to two columns, one clear and one containing the cloud, for each grid box. In our case, we calculate up to 10 columns, one for each cloud type and one clear. Each cloud type is assumed to be a single-layer cloud with a layer thickness given by the same climatology used by Zhang et al. (1995). Co-occurring cloud types do not overlap. These assumptions on the cloud vertical structure may cause the underestimation of the cloud effects on the surface longwave fluxes due to the overestimation on the cloud base heights, but the effect would be notable (but still small; see Chen et al. 1999, manuscript submitted to *J. Climate*) only for cloud types that have systematically larger layer thicknesses than assumed here, such as the deep convective clouds, or for cloud types that frequently occur with another lower-level cloud (cf. Warren et al. 1985).

The specific D1 parameters used for the flux calculation are 1) single-layer cloud parameters specified by the area-averaged cloud fractional cover (Cf), optical thickness ($\tau$), and cloud-top temperature ($T_c$), as well as these same parameters for each of the nine cloud types from the visible/infrared analysis; 2) surface temperature ($T_s$) and visible reflectance ($R_s$) from the ISCCP clear sky composites; and 3) column ozone abundance ($O_3$), atmospheric temperature profile ($T_a$) (up to the 15-mb level), and precipitable water profile (up to 300 mb) originally from the Television Infrared Observational Satellite Operational Vertical Sounder System (Kidwell 1995) but appended in the ISCCP D1 product. Additional datasets used to specify parameters in the radiative transfer model, but not supplied by the ISCCP datasets, are 1) a climatology of cloud layer thickness as a function of cloud-top height, latitude, and season based on rawinsonde and surface observations (Poore et al. 1995; Wang and Rossow 1995); 2) a climatology of aerosol optical thicknesses and compositions adapted from Charlson et al. (1991) for the anthropogenic component and from Toon and Pollack (1976) for the natural background components; 3) latitude and month-dependent ozone profiles from London et al. (1976); 4) global vegetation distribution data and spectral ratios between visible and near-IR albedos for eight vegetation–land surface types and snow/ice as used in the GISS climate GCM (based on Matthews 1983, 1984); 5) a climatology of upper-stratospheric temperatures (15 mb above) from Stratospheric Aerosol and Gas Experiment II (SAGE II;

Liao et al. 1995); and 6) humidity values between 300 and 200 mb from Oort (1983), above the 200-mb level from SAGE II (Liao et al. 1995). Zhang et al. (1995) have conducted a set of sensitivity studies to assess the uncertainties in calculated fluxes caused by the estimated uncertainties in the measurement or specification of the input quantities. The results of their sensitivity studies suggest that the flux uncertainties caused by input data uncertainties would not change the relative magnitude of cloud-type radiative effects, which is the primary purpose of this study.

Comparisons of the earlier version of the ISCCP dataset showed a significant underestimate of cirrus clouds, mostly because they are too optically thin to be detected by ISCCP (Liao et al. 1995; Jin et al. 1996; Stubenrauch et al. 1998a). Although there are other errors, this one is the largest in terms of its effect on cloud cover, so we repeat some calculations to test the importance of the missing cirrus. The test calculations are done by doubling the amount of detected cirrus, whenever present in one map grid box, up to the limit of complete overcast in that grid box. These clouds are added to the detected cirrus assuming that they have the same cloud-top location and a visible optical thickness of 0.2 (approximately the detection limit of ISCCP). As might be expected, the largest change is in the TOA upward longwave fluxes: adding the missing cirrus reduces this flux by $<1$ W m$^{-2}$. All other fluxes change by $<0.3$ W m$^{-2}$.

The output dataset contains all of the radiative flux components. Net fluxes are derived from the corresponding upward and downward flux components: net shortwave fluxes at TOA, at the surface and in the atmosphere ($NS_t$, $NS_s$, $NS_a$); net longwave fluxes at TOA, at the surface and in the atmosphere ($NL_t$, $NL_s$, $NL_a$); and net radiative fluxes (shortwave plus longwave) at TOA, at the surface and in the atmosphere ($N_t$, $N_s$, $N_a$). The in-atmosphere fluxes are determined as differences between the TOA and surface fluxes. All fluxes are calculated for full sky (actual cloud cover), for overcast sky for the mean cloud and the nine individual types (for mean cloud and nine types), and for clear sky. The sign convention of the net fluxes is such that positive values mean heating and negative values mean cooling.

## 4. Radiative effects of different cloud types

The cloud effect on individual radiative flux components will be described by the difference between the flux calculated with and without clouds present, with all other (surface and atmospheric) quantities held fixed for each individual map grid box and time. When this procedure is applied to a net flux or flux divergence, it can properly be thought of as a ''forcing,'' but not when it is applied to a single flux component (Rossow and Zhang 1995). To avoid confusion, we will refer to this quantity as the cloud-induced radiative flux change (hereafter CFC).

The qualitative dependence of the radiative fluxes on cloud characteristics can be inferred from previous studies of the effects of total cloudiness (see Hartmann et al. 1992; Rossow and Zhang 1995 and references therein). For example, high-level clouds are most effective in altering TOA upward longwave fluxes (commonly called outgoing longwave radiation) because they are relatively colder than the surface and lower atmosphere, whereas low-level clouds have little effect because they have a similar temperature. However, for the same reasons, the reverse is true for surface downward longwave fluxes. Optically thin clouds like cirrus or cumulus have only a small effect on either TOA upward or surface downward shortwave fluxes, while optically thick clouds like nimbostratus have a larger effect. However, the actual radiative importance of each cloud type is also controlled by their relative abundance (the product of their typical areal coverage and their frequency of occurrence, here called cloud amount). To separate the radiative effects caused by the variations in radiative properties of each cloud type from that caused by the variations in their abundance, we first consider the CFC produced when the cloud cover for each cloud type is assumed to be complete (overcast sky). Furthermore, by holding the radiative properties fixed and factoring out the effects caused by the relative abundance for each cloud type, the geographical and seasonal variations in the overcast sky calculations also demonstrate the equally important roles played by surface and atmospheric properties in determining the cloud effects on various radiative flux components. These overcast sky values of CFC for a given cloud type can be considered as the cloud-induced change in the radiative flux per unit area (where our fractions are for areas of $\approx$78 000 km$^2$), similar to the sensitivity coefficient of Hartmann et al. (1992). To illustrate some of the regional variability caused both by regional variations of the cloud properties and regional differences in the surface and atmospheric properties (cf. Zhang et al. 1995; Rossow and Zhang 1995), we examine zonal mean values of CFC (a more detailed examination of the land–ocean contrast of CFC values for different cloud types should be considered later). Then we calculate the CFC values when the cloud cover is the observed amount for that cloud type (full sky) to determine which cloud types have the most important effects on the radiation budget.

As mentioned before, the calculation of statistically accurate, climatological CFC values for each cloud type was not possible because the whole procedure is very time consuming. Rather, the purpose of this study is to obtain representative estimates of the cloud-type CFC values. Therefore, we perform calculation on one day of data from each of the four seasons to get a representative mix of situations and, to save space, show only the 4-day average results, approximating the annual mean (except that the results in the polar regions do not have a contribution from the winter season when the complete cloud-type information is not available in the

absence of sunlight). These ''annual'' mean CFC values are relevant to the possible cloud–radiative feedbacks on long-term climate change. In the last part of this section, we discuss the seasonal variations of the full sky CFC values to consider feedbacks on the seasonal cycle and the hemispheric differences that arise.

### *a. Annual mean overcast sky CFCs*

#### 1) AT TOA AND AT THE SURFACE

Figure 3 shows the annual, zonal mean overcast sky CFC values for the net TOA shortwave (CFC-$NS_t$) and longwave (CFC-$NL_t$) for the nine different cloud types. Also shown are the average CFC values for high, middle, and low clouds; the average for optically thin, medium and thick clouds; and the average over all cloud types. Figure 4 shows the same at the surface (CFC-$NS_s$, CFC-$NL_s$). The global mean values from these figures are summarized in Table 1. Note that in all the CFC plots (from Figs. 3 to 10), polar regions are shown using dashed lines, since in the flux calculations, polar regions are excluded during winter seasons when the cloud type information is unavailable. Thus, to make these 4-day averaged CFC plots extend to the Poles, we set the CFCs to be zero whenever they are not available. But for the global mean values, the polar regions are simply left out during winter seasons. Although the winter seasons are excluded near the Poles, the global mean CFC values are only slightly biased considering the small-areal coverage of polar regions. In the absence of sunlight and with the frequent occurrence of near-surface temperature inversions, the wintertime shortwave CFC values are zero and the longwave CFC values are $+10$–$20$ W m$^{-2}$ (cf. Curry et al. 1996) implying that the shortwave CFCs are exact, whereas the longwave CFCs are underestimated by a few watts per square meter near the Poles in the plots. The contribution of the winter season to the annual mean is small.

The shortwave CFC values (negative values indicate a net cooling effect) are very similar in magnitude at TOA and at the surface with little variation with latitude.[1] The optically thinnest clouds ($\tau \leq 3.6$) produce shortwave CFC $\approx -25$ W m$^{-2}$ at both TOA and at the surface, while the thicker clouds ($\tau > 3.6$) produce values $\approx -100$ W m$^{-2}$ at both TOA and at the surface. The average shortwave CFC is about the same for clouds at all levels, though there is a progressive increase with height because the mean optical thickness increases with height; a more accurate treatment of the high-level ice clouds would enhance this increase slightly. The small latitudinal variations for each cloud type indicate some variation of the mean properties of the cloud types, but the hemispheric asymmetry is caused by the lower surface albedo in the predominantly ocean-covered Southern Hemisphere relative to the predominantly land-covered Northern Hemisphere. The near independence of the overcast CFC-$NS_t$ and CFC-$NS_s$ with latitude, even though the annual mean solar insolation peaks at the equator, is caused by the increase of cloud albedo with decreasing solar zenith angle (Rossow and Zhang 1995); however, this effect is probably weaker when the scattering by ice clouds is correctly treated. Overall, the largest-magnitude shortwave CFC is produced by the cloud types with the largest mean cloud optical thicknesses; namely, stratus, nimbostratus, and deep convective (Table 1). There is a systematic increase of the mean optical thickness with cloud-top height among these three cloud types.

The longwave CFC values (positive values indicate a net heating effect) at TOA are largest for high-level clouds near the equator ($>70$ W m$^{-2}$) where the cloud tops are highest and their temperature contrast with the surface is largest, while the CFC of low-level clouds is $<10$ W m$^{-2}$. On the other hand, longwave CFC values at the surface are largest (almost 50 W m$^{-2}$) for low-level clouds at higher latitudes where the longwave opacity of water vapor is smaller. Near the equator where the water vapor opacity is largest, the low-level longwave CFC falls below 20 W m$^{-2}$. Overall the contrast between the high-level and low-level longwave CFC values is smaller at the surface than at TOA. Since longwave emission and transmission effects of clouds ''saturate'' at relatively low (visible) optical thicknesses, the longwave CFC is noticeably different only for the optically thinnest cloud types. The general latitude dependence is related to decreasing temperatures and humidity with latitude; the hemispheric asymmetry arises from the fact that the annual mean temperature and humidity are smaller in the Southern than in the Northern Hemisphere. Overall, the largest longwave CFC at TOA is produced by cirrostratus and deep convective clouds; the largest longwave CFC at the surface is produced by stratocumulus and stratus (Table 1).

Figure 5 shows the annual, zonal mean CFC values for the total net flux (shortwave plus longwave). Although the shortwave CFC values can be said to be generally larger in magnitude than the longwave CFC values, so that the total net CFC is generally negative, this figure reveals significant differences of the total net CFC between TOA and the surface as a function of latitude that vary systematically among the different cloud types. The values of CFC-$N_t$ for low- and midlevel clouds generally follow those of their CFC-$NS_t$ values because they are much larger than the corresponding values of CFC-$NL_t$.

At TOA, the total net CFC is negative at almost all latitudes (Fig. 5); however, the total CFC can be positive near the Poles (adding the wintertime contribution increases the total CFC). The cirrus total net CFC (not shown) is positive (about 10 W m$^{-2}$ heating in the Trop-

[1] The discussion of the latitudinal variations of CFCs in the text only applies to the latitudinal bands where cloud-type observations are available year-round; namely, 57.5°S–57.5°N.

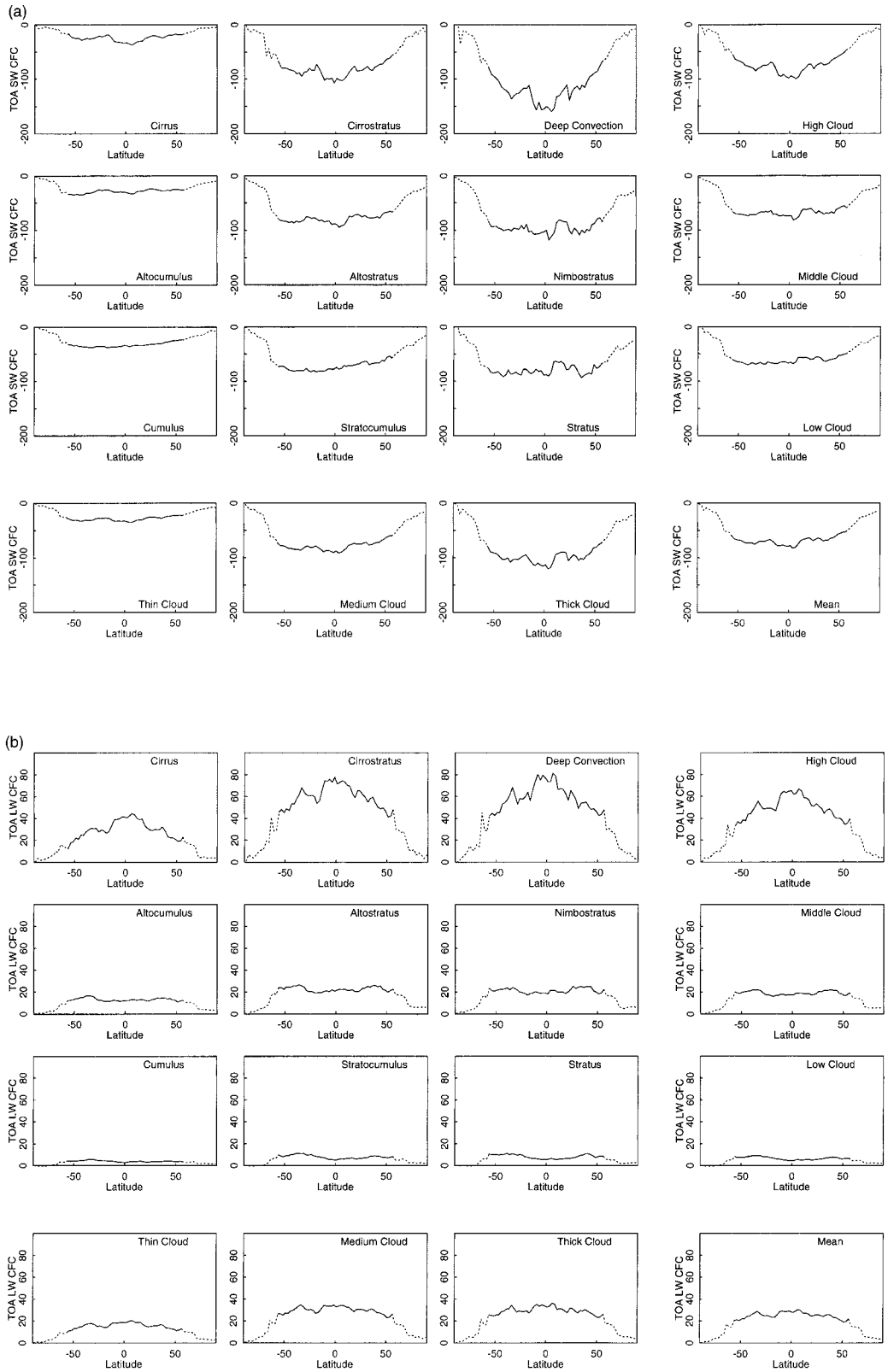


FIG. 3. (a) Annual (4-day average), zonal mean overcast sky CFC values (W $m^{-2}$) for the net TOA shortwave (CFC-$NS_t$) for the nine different cloud types (see section 2 for definition of acronyms), along with averages for three cloud-top height (high, middle, and low clouds) and optical thickness categories (optically thin, moderate, and thick clouds), and average for all the nine cloud types. (b) Same as (a), but for the net TOA longwave CFC (CFC-$NL_t$).

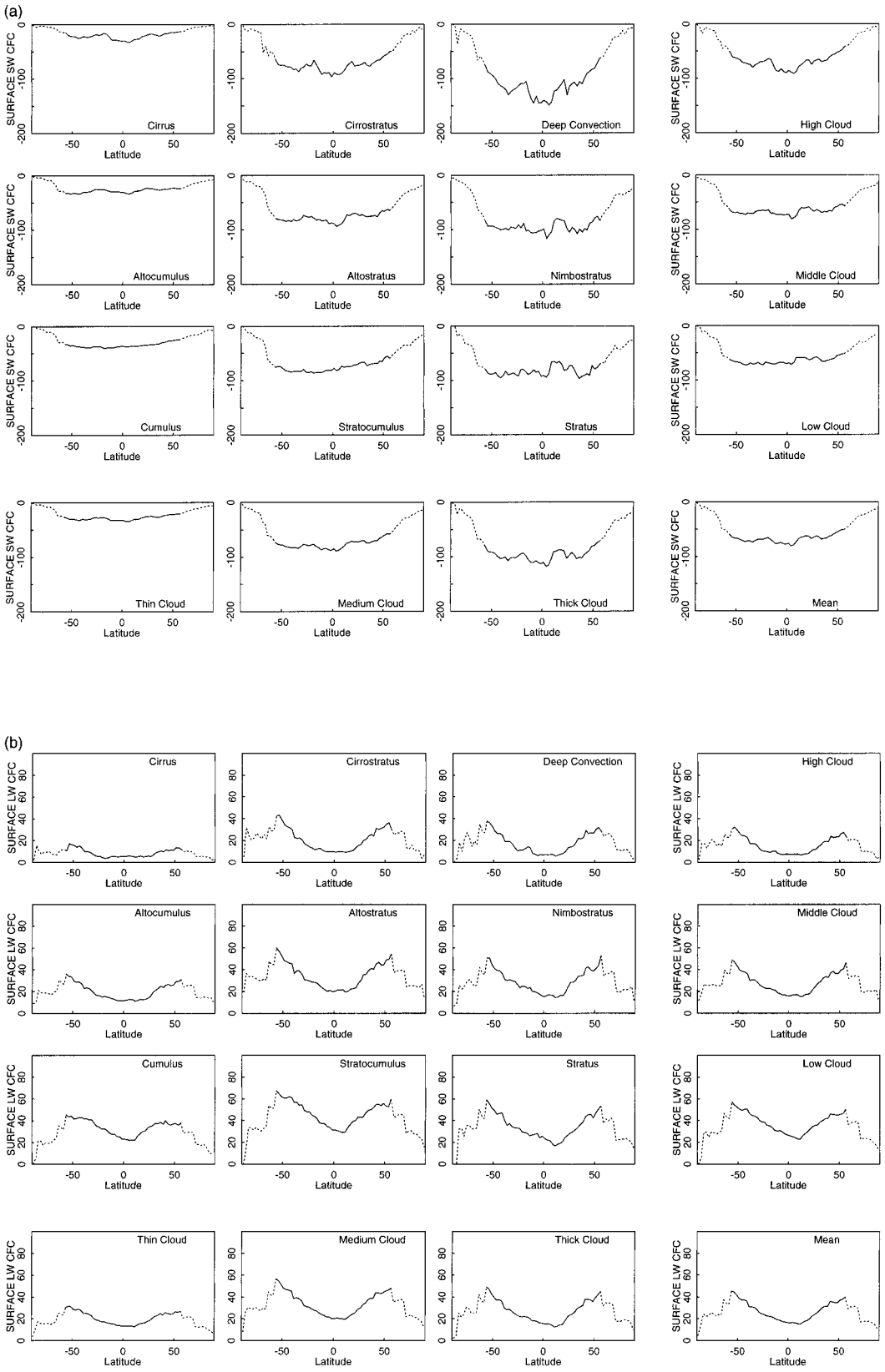


FIG. 4. (a) Same as Fig. 3a, but for the net surface shortwave CFC (CFC-$NS_s$). (b) Same as Fig. 3a, but for the net surface longwave CFC (CFC-$NL_s$).

TABLE 1. Global annual (4-day averaged) mean overcast sky cloud-induced radiative flux changes in W $m^{-2}$ at the surface, at TOA, and in-atmosphere. SW—shortwave, LW—longwave, and TL—total.

| | Surface | | | TOA | | | Atmosphere | | |
|---|---|---|---|---|---|---|---|---|---|
| Cloud type | SW | LW | TL | SW | LW | TL | SW | LW | TL |
| Cirrus | −22.2 | 8.0 | −14.2 | −25.3 | 30.7 | 5.4 | −3.1 | 22.7 | 19.6 |
| Cirrostratus | −79.5 | 20.0 | −59.5 | −87.4 | 59.7 | −27.7 | −7.9 | 39.7 | 31.8 |
| Deep convective | −118.6 | 16.3 | −102.3 | −126.2 | 60.7 | −65.5 | −7.6 | 44.4 | 36.8 |
| Altocumulus | −28.7 | 20.3 | −8.4 | −29.3 | 13.0 | −16.3 | −0.6 | −7.3 | −7.9 |
| Altostratus | −79.6 | 35.4 | −44.2 | −80.9 | 22.1 | −58.8 | −1.3 | −13.3 | −14.6 |
| Nimbostratus | −98.2 | 32.4 | −65.8 | −98.8 | 20.6 | −78.2 | −0.6 | −11.8 | −12.4 |
| Cumulus | −35.4 | 33.4 | −2.0 | −33.8 | 4.0 | −29.8 | 1.6 | −29.4 | −27.8 |
| Stratocumulus | −77.7 | 46.8 | −30.9 | −74.7 | 7.7 | −67.0 | 3.0 | −39.1 | −36.1 |
| Stratus | −88.1 | 39.2 | −48.9 | −84.6 | 7.8 | −76.8 | 3.5 | −31.4 | −27.9 |

ics). Although the magnitude of the effect of the very thin cirrus missed by the ISCCP analysis is very small, the experiment of adding the missing cirrus as described in section 3 shows that it would slightly decrease the overcast cirrus total net CFC. The overcast CFC-$N_t$ for deep convective clouds (not shown) is actually slightly larger (−65 W $m^{-2}$) than for mid- and low-level clouds, because of a much larger mean optical thickness and despite their large values of CFC-$NL_t$, consistent with Hartmann et al. (1992).

At the surface, the total net CFC is generally larger (less negative) than at TOA (Fig. 5). The net cirrus CFC (not shown) is still negative at low latitudes because their longwave effect on the surface is blocked by high water vapor opacity. The net CFC for deep convective clouds (not shown) is larger in magnitude at the surface than at the TOA because its longwave effect is much smaller at the surface than at the TOA (but note that in these calculations, the cloud base assumed for the deep convective cloud type using the general climatology of cloud layer thicknesses is probably much too high; correcting this error would reduce the magnitude of its total net CFC but will not change the sign of it). Overall, the net negative effect of clouds on the net surface radiation decreases poleward (Fig. 5); in fact, the total net CFC for low-level clouds becomes positive at higher latitudes, especially for cumulus (optically thin) (not shown), because low annual mean solar insolation reduces their shortwave CFC and low water vapor opacity increases their longwave CFC relative to low-latitude clouds. On average, the dominant contributions to the negative total net CFC come from the nimbostratus and deep convective clouds (not shown).

### 2) IN-ATMOSPHERE

A unique aspect of our analysis approach is that it allows for an estimate of the cloud effects on the net radiation absorbed by the atmosphere in a physically consistent manner (Zhang et al. 1995). Figure 6 shows annual, zonal mean, in-atmosphere net shortwave (CFC-$NS_a$), and net longwave (CFC-$NL_a$) overcast CFC for the nine cloud types, along with averages for three cloud-top height and optical thickness categories.

Averaged over all the cloud types, the shortwave CFC is about −1 W $m^{-2}$; however, this result arises from the mixture of low-level clouds with positive CFC values and high-level clouds with negative CFC values with midlevel clouds having CFC values near zero (Fig. 6a). The magnitude of the CFC increases with optical thickness at both levels. The change in sign of the net shortwave CFC with cloud-top height is produced by the

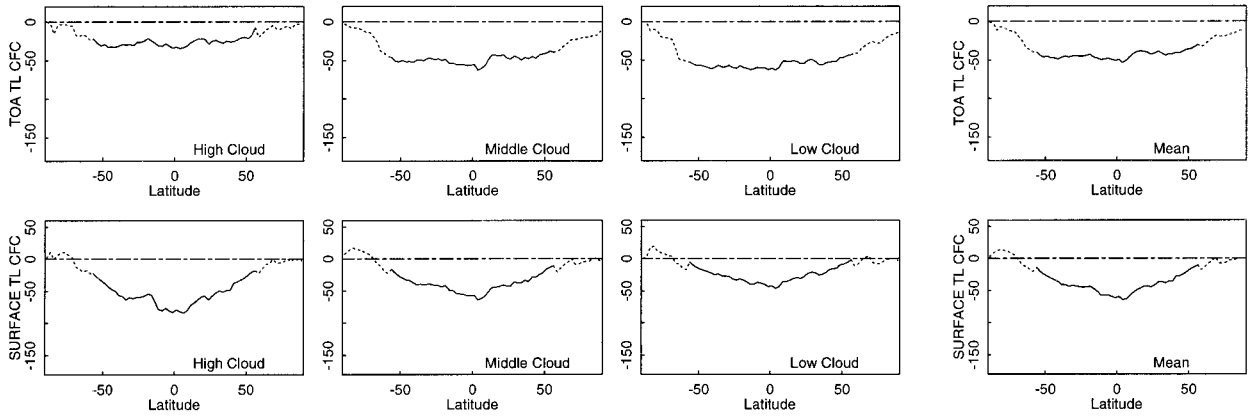


FIG. 5. Annual, zonal mean overcast sky CFC values (W $m^{-2}$) for the total (shortwave plus longwave) net TOA (CFC-$N_t$) and total (shortwave plus longwave) net surface (CFC-$N_s$) for high, middle, low, and all clouds.

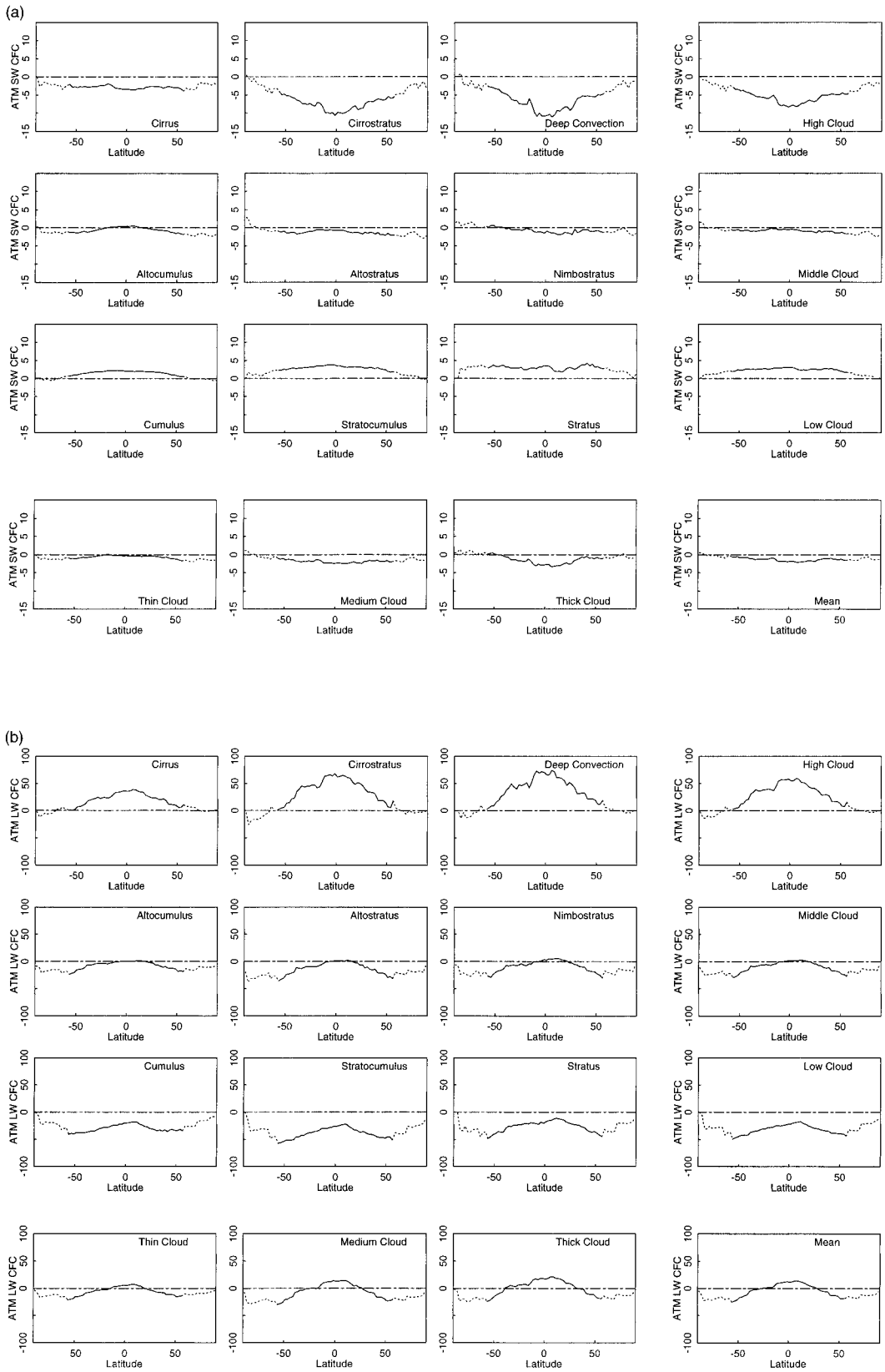


FIG. 6. (a) Same as Fig. 3a, but for the net in-atmosphere shortwave CFC (CFC-$NS_a$). (b) Same as Fig. 3a, but for the net in-atmosphere longwave CFC (CFC-$NL_a$).

changing balance among three offsetting contributions to total shortwave absorption by the atmospheric column. 1) Adding clouds to the column increases the upward shortwave flux because of their higher albedo than the surface, consequently increasing the shortwave absorbed by water vapor and ozone above the clouds; 2) adding clouds to a layer increases the shortwave absorbed there because clouds absorbs more near-IR radiation than water vapor and because clouds increase the average photon path length by scattering; and 3) adding clouds shields the water vapor below thereby decreasing the shortwave absorbed below the cloud (Rossow and Zhang 1995). For low-level clouds, the first two effects surpass the third one, causing increased atmospheric shortwave absorption; for high-level clouds, the third effect surpasses the first two, causing decreased atmospheric shortwave absorption (the three effects nearly cancel for midlevel clouds). With an improved treatment of ice clouds, the magnitude of the high-level cloud CFC will increase slightly. Although the net shortwave CFC values are small for the whole atmospheric column, all of the clouds, including midlevel ones, significantly change the vertical distribution of total absorbed shortwave in the atmosphere that can affect the atmospheric circulation (cf. Webster and Stephens 1984; Chen et al. 1999, manuscript submitted to *J. Climate*). Overall, the largest-magnitude shortwave CFC in the atmosphere, which is a cooling effect, is produced by cirrostratus and deep convective clouds; of the clouds that produce a heating effect, the largest one is produced by stratocumulus and stratus.

The in-atmosphere longwave CFC values (Table 1; Fig. 6b) are generally much larger in magnitude than the shortwave CFC values; but, in contrast to the shortwave, low-level clouds (and midlevel clouds at higher latitudes) cause increased longwave cooling of the atmosphere, while high-level clouds cause decreased longwave cooling (a heating effect). The reason for this arises from a changing balance of two offsetting effects. 1) Adding clouds decreases the atmospheric longwave cooling by decreasing its effective emission temperature, and 2) adding clouds increases the atmospheric longwave cooling by increasing the effective emissivity of the atmosphere in the water vapor window (8–14-$\mu$m wavelength). The latter effect becomes more important at higher latitudes where there is less water vapor opacity than in the Tropics (Rossow and Zhang 1995). For high-level clouds, the first effect exceeds the second one, especially in the Tropics where the second effect is rather small; for low-level clouds, the second effect exceeds the first one since low-level clouds are relatively inefficient in decreasing the effective emission temperature. For midlevel clouds, the two opposing effects almost completely cancel in the Tropics. As with the shortwave, the changes even for midlevel clouds are important because they still cause a vertical redistribution of the atmospheric cooling, even if their net effect on the total atmospheric column is small (Chen et al. 1999, manuscript submitted to *J. Climate*). The latitudinal variations of overcast CFC-$NL_a$, which are larger than for the shortwave, are caused mostly by varying water vapor opacity. Overall, the largest-magnitude longwave CFC in the atmosphere is produced by cirrostratus and deep convection, a heating effect that peaks near the equator, and by stratocumulus, a cooling effect that peaks at the Poles.

The behavior of the cloud effect on the total net atmospheric flux (CFC-$N_a$; not shown) follows that of the much larger longwave component. The total average overcast effect of clouds on the earth's radiation budget (Fig. 5), which is an overall latitude-independent cooling compared with a clear atmosphere with the same properties, is divided into a strong net cooling of the low-latitude surface, a heating of the tropical atmosphere, and a cooling of the high-latitude atmosphere. If all of the clouds had the properties of cirrus clouds, they would cause a slight overall heating, a significant atmospheric heating offset by surface cooling at lower latitudes. If all of the clouds had the properties of deep convective clouds, the overall effect would be a strong cooling, appearing mostly at the surface and offset by some atmospheric heating. If all clouds were cumulus, a weak surface cooling at lower latitudes is reinforced by weak atmospheric cooling, whereas weak surface heating at higher latitudes is offset by stronger atmospheric cooling, to produce a weak net cooling of the earth at all latitudes. Finally, if all clouds were stratus, strong surface cooling is reinforced by atmospheric cooling, which is weaker near the equator than at the Poles, to produce strong cooling of the earth.

### *b. Annual mean full sky CFCs*

In the previous section we have shown how the variation of the radiative effects of clouds depends on their top height and optical thickness, which are used to define the cloud types. As expected, the largest effects on shortwave fluxes are produced by adding clouds with the largest optical thicknesses and the largest effects on the longwave fluxes at TOA (or surface) are produced by adding clouds with the highest (or lowest) cloud-top heights. However, the actual relative importance of each of these cloud types in the current climate's radiation budget also depends on their abundance. Figure 1 shows the annual, global mean amounts and Fig. 2 shows the annual, zonal cloud-type amounts. The latitude variations of monthly mean high-level cloud amounts from ISCCP agree to within 0.05 rms with the climatology based on surface observations (Warren et al. 1986, 1988) and, although the ISCCP mid- and low-level clouds are lower by 0.15–0.20 than the surface climatology values as expected from the top-down satellite viewpoint, the net effect on surface radiative fluxes is small (Zhang et al. 1995). When discussing the relative contributions of different cloud types, the relative importance of low-level clouds is underestimated somewhat. Several fea-

tures are apparent in Fig. 1. 1) The three most abundant cloud types are cumulus, cirrus, and stratocumulus, which account for 58% of the total cloudiness (0.37 out of a total cloud fraction of 0.63). (Note that the cloud fraction numbers quoted in the text are the 4-day averaged values, but the numbers in Fig. 1 are from the 5-yr climatology.) 2) Most clouds have $\tau \leq 23$; less than 10% of all clouds have $\tau > 23$. 3) Low-level clouds occur most of the time (41%, despite the satellite underestimate); midlevel clouds occur the least (25%), and high-level clouds occur 34% of the time. 4) The latitudinal pattern of total high-level cloud fraction shows the major storm zones more clearly than any other cloud-type group. 5) The fraction of midlevel and low-level clouds is smaller in the Tropics, where high-level clouds are abundant, so that this result might be influenced by the top-down satellite viewpoint.

#### 1) AT TOA AND AT THE SURFACE

Figures 7 and 8 show the annual, zonal mean full sky CFC values (CFC-$NS_t$, CFC-$NL_t$, CFC-$NS_s$, and CFC-$NL_s$) at TOA and at the surface for the nine cloud types, where each value is now weighted by its actual cloud amount as a function of latitude (cf. Fig. 2). Table 2 gives the corresponding global mean values. Since the cloud amounts are all less than unity, all of the CFC values in W $m^{-2}$ are much smaller than shown in Figs. 3 and 4 (cf. values in Tables 1 and 2). The results for each of three optical thickness and three cloud-top height categories are sums of the corresponding cloud-type CFC values. Comparing with the overcast sky results (Figs. 3 and 4), the latitude variations of all the CFC values for high-level clouds, except for CFC-$NL_s$, are larger because this type of cloud exhibits the most latitudinal variation of cloud amount. However, the full sky CFC-$NS_t$ and CFC-$NS_s$ values for low-level clouds also vary more than for the overcast values. Overall, the most important cloud types for the shortwave CFC are those with moderate optical thicknesses—namely stratocumulus, altostratus, and cirrostratus—rather than the types with the largest optical thicknesses. In other words, the differences in cloud amount more than offset the differences in optical thickness. These three cloud types account for 38% of the total cloudiness but produce 54% of the full sky CFC-$NS_t$ ($-29$ W $m^{-2}$ out of a total of $-54$ W $m^{-2}$) and 55% of the full sky CFC-$NS_s$ ($-29$ W $m^{-2}$ out of the total $-53$ W $m^{-2}$). The fractional contributions to the shortwave CFC values are roughly the same for high-, mid-, and low-level cloud.

For the full sky CFC-$NL_t$, the three most important cloud types are still the high-level clouds—namely, cirrus, cirrostratus, and deep convective cloud—but the contribution of cirrus is now larger than that of deep convection and similar to that of cirrostratus. High-level clouds account for 33% of the total cloudiness but produce 69% of the full sky CFC-$NL_t$ (14 out of a total of 20 W $m^{-2}$). For the full sky CFC-$NL_s$, the three most important cloud types are cumulus, stratocumulus, and altostratus. Because of the different cloud amounts, a midlevel cloud type now contributes more to the surface longwave CFC than the stratus clouds, especially at higher latitudes. The cumulus, stratocumulus, and altostratus account for 35% of the total cloudiness but produce 66% of the full sky CFC-$NL_s$ (16 W $m^{-2}$ out of the total 24 W $m^{-2}$).

Figure 9 shows the total net (shortwave plus longwave) CFC values at TOA and at the surface. The global mean total net CFC is $-33$ W $m^{-2}$ at TOA and $-28$ W $m^{-2}$ at the surface, indicating the dominance of the shortwave CFC (these values are within 1–2 W $m^{-2}$ of those given by Rossow and Zhang 1995). At the TOA, the cloud effect is larger at higher latitudes than near the equator. Low-level clouds contribute about half of the total cloud effect, whereas high clouds contribute less than a quarter of it; moderate optical thickness cloud types contribute about 60% of the global total, and thin clouds contribute less than 20% (not shown). Overall, the three most important cloud types at TOA are stratocumulus, altostratus, and cumulus. At the surface (Fig. 9), the cloud effect peaks in the Tropics, where half of it is contributed by high-level clouds. Overall, the three most important types at the surface are stratocumulus, cirrostratus, and deep convective clouds (given that we probably place the base of deep convective clouds at too high altitude, altostratus may actually be slightly more important to the total net CFC at the surface). Cirrus is notable because it has net CFC value at TOA that is opposite in sign to the generally negative values of the other cloud types (not shown): cirrus causes a small net heating at TOA (but since cirrus cause a small net cooling at the surface, this heating appears in the atmosphere as we discuss next).

#### 2) IN-ATMOSPHERE

Figure 10 shows the annual, zonal mean net CFC for full sky (CFC-$NS_a$ and CFC-$NL_a$). Overall, clouds reduce the atmospheric shortwave heating and increase the longwave cooling slightly, resulting in 5 W $m^{-2}$ more cooling (compared with the clear sky value) in the global mean (Table 2). However, there is strong latitudinal dependence of the longwave net CFC (dominant component): adding clouds heats the tropical atmosphere and cools the high-latitude atmosphere (Fig. 10b; cf. Rossow and Zhang 1995). Examining Fig. 10 more closely shows that these small global mean effects are comprised of important redistributions of the atmospheric heating/cooling. If all the clouds were low level, there would be a net shortwave heating effect on the atmosphere; the larger shortwave cooling effect of high-level clouds offsets the low-level cloud effect and indicates that the total shortwave heating in the atmosphere has been shifted to higher levels by the clouds. The reverse situation occurs in the longwave radiation:

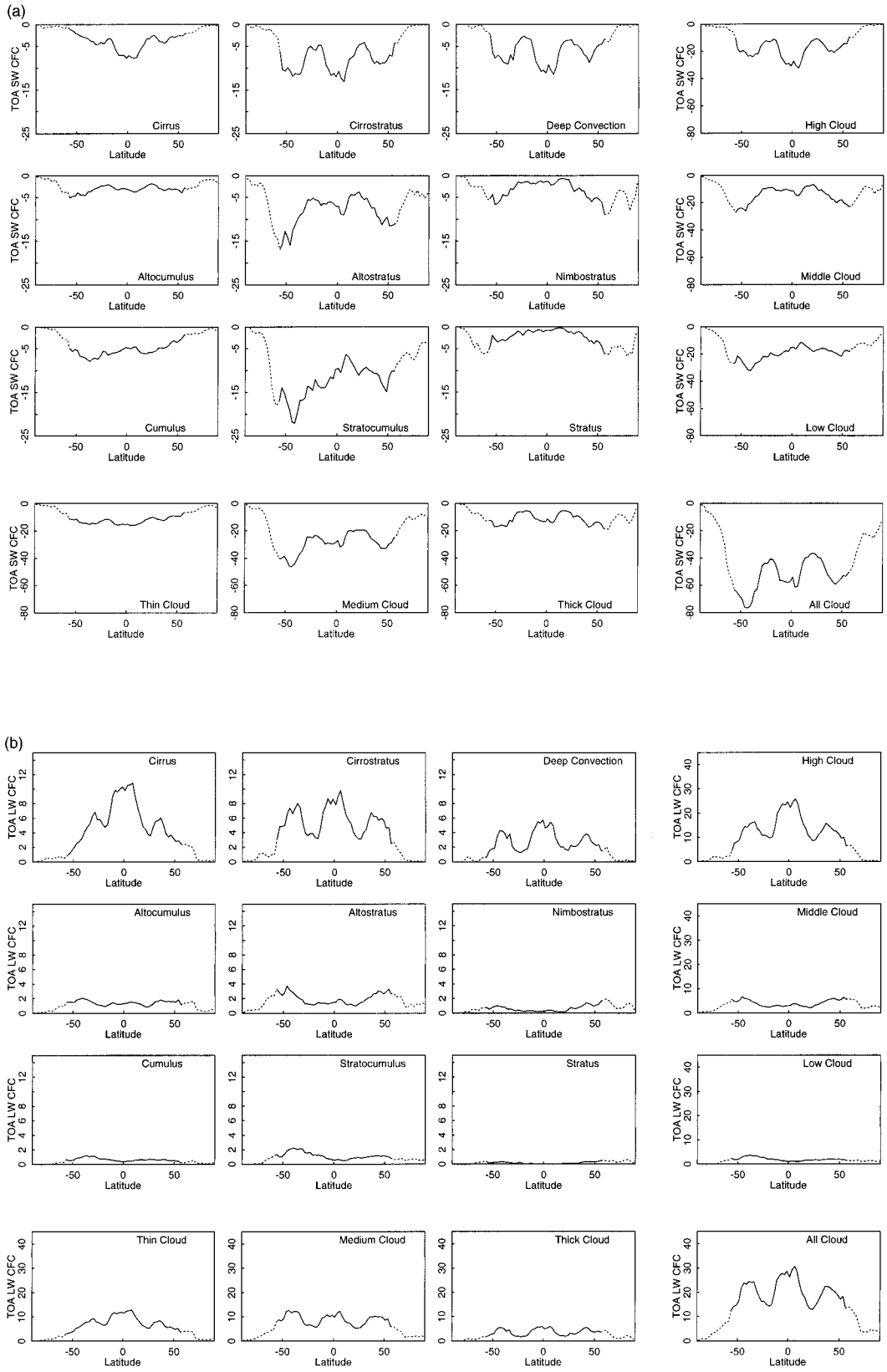


FIG. 7. (a) Annual, zonal mean full sky CFC values (W $m^{-2}$) for the net TOA shortwave (CFC-$NS_t$) for the nine different cloud types (see section 2 for definitions); also shown are the overall CFC values for high, middle, and low clouds and for optically thin, moderate, and thick clouds, as well as the overall CFC values for all clouds. (b) Same as (a), but for the net TOA longwave CFC (CFC-$NL_t$).

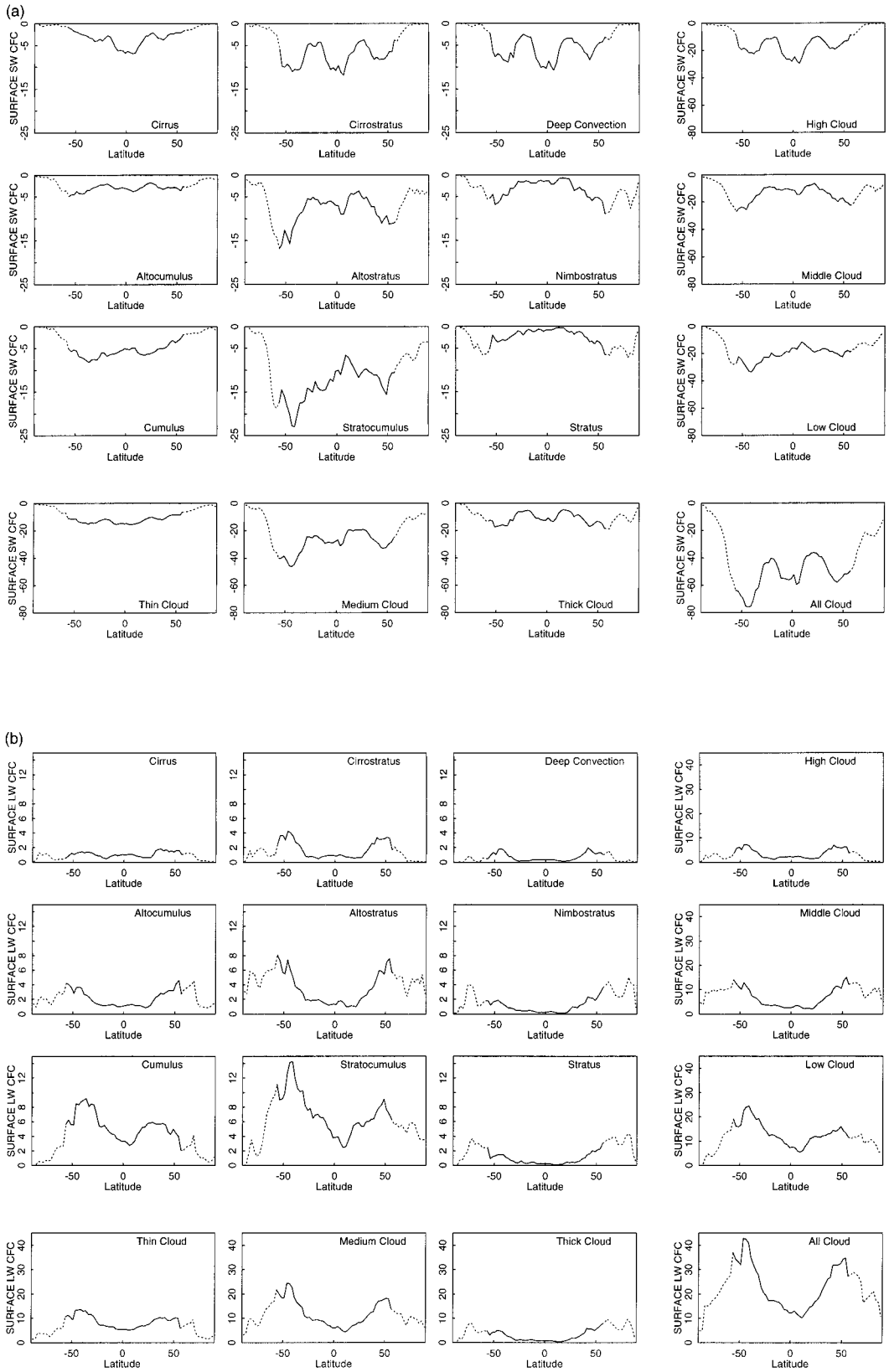


FIG. 8. (a) Same as Fig. 7a, but for the net surface shortwave CFC (CFC-$NS_s$). (b) Same as Fig. 7a, but for the net surface longwave CFC (CFC-$NL_s$).

TABLE 2. Global annual mean full sky cloud-induced radiative flux changes in W m$^{-2}$ at the surface, at TOA, and in-atmosphere. The names of three most abundant cloud types are shown in bold.

| | Surface | | | TOA | | | Atmosphere | | |
|---|---|---|---|---|---|---|---|---|---|
| Cloud type | SW | LW | TL | SW | LW | TL | SW | LW | TL |
| **Cirrus** | −3.6 | 1.1 | −2.5 | −4.2 | 5.5 | 1.3 | −0.6 | 4.4 | 3.8 |
| Cirrostratus | −7.2 | 1.7 | −5.5 | −7.9 | 5.5 | −2.4 | −0.7 | 3.8 | 3.1 |
| Deep convective | −5.8 | 0.7 | −5.1 | −6.2 | 2.9 | −3.3 | −0.4 | 2.2 | 1.8 |
| Altocumulus | −3.1 | 2.2 | −0.9 | −3.2 | 1.5 | −1.7 | −0.1 | −0.7 | −0.8 |
| Altostratus | −8.2 | 3.6 | −4.6 | −8.3 | 2.0 | −6.3 | −0.1 | −1.6 | −1.7 |
| Nimbostratus | −3.4 | 1.3 | −2.1 | −3.4 | 0.7 | −2.7 | 0.0 | −0.6 | −0.6 |
| **Cumulus** | −5.5 | 5.3 | −0.2 | −5.2 | 0.6 | −4.6 | 0.3 | −4.7 | −4.4 |
| **Stratocumulus** | −13.2 | 7.3 | −5.9 | −12.7 | 1.2 | −11.5 | 0.5 | −6.1 | −5.6 |
| Stratus | −2.6 | 1.2 | −1.4 | −2.4 | 0.2 | −2.2 | 0.2 | −1.0 | −0.8 |
| Sum (true) | −52.6 | 24.4 | −28.2 | −53.5 | 20.1 | −33.4 | −0.9 | −4.3 | −5.2 |

low-level clouds alone would cool the atmosphere by inhibiting radiative exchanges with the surface, and high-level clouds alone would heat the atmosphere by inhibiting radiative exchanges with space. The latter effect prevails in the Tropics, caused mostly by cirrus and cirrostratus clouds, whereas the former effect prevails at higher latitudes, caused mostly by stratocumulus clouds and enhanced by the increased effective emissivity under drier conditions.

### *c. Seasonal variations of full sky CFC*

At both TOA and the surface, the total CFC for the optically thicker cloud types reaches a minimum (most negative value) near 60° latitude in the summer hemisphere because of the predominance of the shortwave CFC and the seasonal redistribution of solar illumination. Since there is no sunlight at the winter pole, the total net CFC is just the longwave CFC, which is positive (Rossow and Zhang 1995), so the total net CFC attains its maximum at the winter pole. In the equinoctial months, the total net CFC attains its minimum near the equator with maxima at both poles. The latitudinal contrast of the total net CFC tends to be larger at the surface than at TOA because varying water vapor opacity with latitude enhances the latitudinal changes of the longwave CFC. The optically thinnest cloud types exhibit a more nearly constant total net CFC with latitude because their shortwave CFC values are much smaller. Note that the shortwave CFC of cirrus is large enough at higher latitudes in the summer hemisphere to make the total net CFC negative at TOA even for this cloud type; the cirrus net CFC is negative at the surface near the equator in all seasons.

The seasonal variations occur mostly because of the seasonal variations in the shortwave CFC values, largely as a result of changing solar zenith angle and daylight duration (Harrison et al. 1990; Rossow and Zhang 1995). The magnitude of the shortwave CFC values is maximum in the summer hemisphere and minimum in winter hemisphere. However, the longwave CFC values are larger in the winter hemisphere than in the summer hemisphere, especially at the surface, suggesting that changes in water vapor opacity are important in determining the magnitude of the cloud effects. The seasonal variations of the longwave CFC reinforce those of the shortwave CFC. As a consequence, cloud systems act against seasonal warming (cf. Harrison et al. 1990). Because the surface albedo is lower in the Southern Hemisphere, the seasonal amplitude of the shortwave CFC

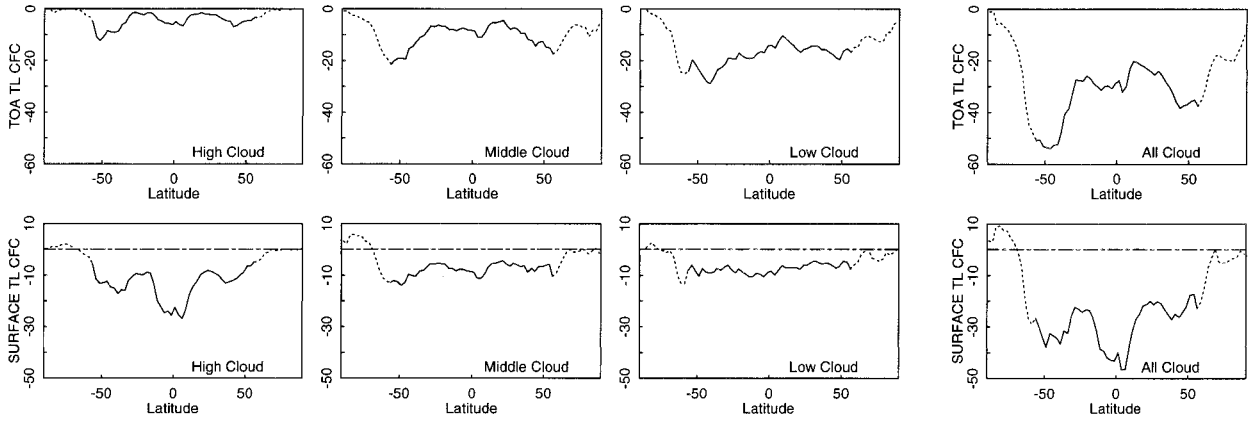


FIG. 9. Same as Fig. 5, but for full sky CFC values (W m$^{-2}$).

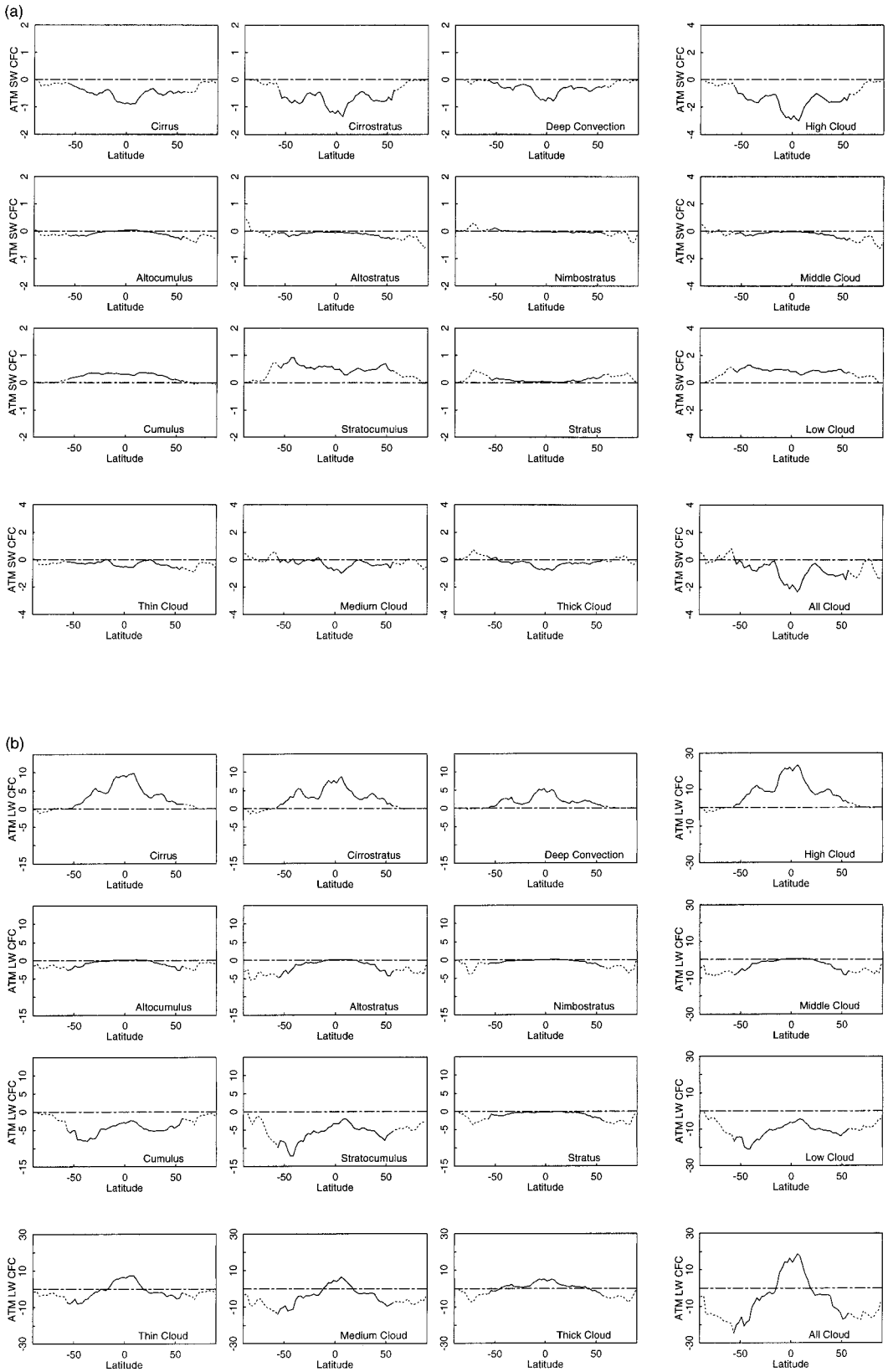


FIG. 10. (a) Same as Fig. 7a, but for the net in-atmosphere shortwave CFC (CFC-$NS_a$). (b) Same as Fig. 7a, but for the net in-atmosphere longwave CFC (CFC-$NL_a$).

values is larger there; likewise, because the seasonal variations of the temperature and humidity are larger in the Northern Hemisphere, the seasonal amplitude of the longwave CFC value is larger there. Because of their large shortwave effect, the thickest cloud types have the largest seasonal CFC variations. The seasonal changes of the in-atmosphere CFCs mostly result from the relative changes of cloud height with the atmospheric longwave effective emission level due to the seasonal variations of humidity.

## 5. Discussion and conclusions

The simplest result we have illustrated by comparing the overcast sky calculations with the full sky calculations is that variations of cloud-top height and optical thickness, expressed in terms of changing cloud type, are just as important as total cloud cover variations in determining the radiation budget. The second result is that different cloud types are most effective in altering the fluxes depending on whether we consider shortwave or longwave fluxes and whether we consider TOA, surface, or in-atmosphere fluxes. These two points together also mean that the importance of treating the radiative effects of a particular cloud type accurately changes depending on the problem. For example, the contribution of deep convective clouds to the total radiation budget is small due to their relatively small abundance. However, when deep convective clouds occur, their radiative effect is large and might be important for the evolution of convective cloud systems (Machado and Rossow 1993). With the cloud properties fixed for each type in the overcast sky calculations, their latitudinal, hemispheric, and seasonal variations also illustrate the delicate interplay among cloud, surface, and atmospheric properties; that is, the same cloud does not produce the same flux changes when the circumstances are different (Rossow and Zhang 1995). All of these results mean that preaveraging the cloud properties before determining their radiative effects can bias the results (see appendix).

With a uniform mix of cloud types, the three cloud types that produce most of the total cloud effect on the TOA shortwave fluxes are (in descending order; see Table 1) deep convective, nimbostratus, and cirrostratus; and for the surface shortwave effect, the three most important cloud types are the three thickest cloud types—namely, deep convective, nimbostratus, and stratus. With a realistic mix of cloud types (Table 2), the cloud types that produce most of the total cloud effect on the shortwave fluxes (both TOA and surface) are (in descending order) the three cloud types with moderate optical thicknesses: stratocumulus, altostratus, and cirrostratus.

With a uniform mix of cloud types (Table 1), the three cloud types that produce most of the total cloud effect on the TOA longwave fluxes are the three high-level cloud types (in descending order), deep convective, cirrostratus, and cirrus; and for the surface longwave effect, the three most important cloud types are stratocumulus, stratus, and altostratus. With a realistic mix of cloud types (Table 2), the three cloud types that produce most of the total cloud effect on the TOA longwave fluxes are still the three high-level cloud types, but in a different order, cirrus, cirrostratus, and deep convective; but for the surface longwave effect, the three most important cloud types are stratocumulus, cumulus, and altostratus.

With a uniform mix of cloud types (Table 1), the three cloud types that produce most of the total cloud effect on the in-atmosphere shortwave fluxes are (in descending order) cirrostratus, deep convective, and stratus, with the former two cloud types decreasing the shortwave heating and the last one increasing the shortwave heating. With a realistic mix of cloud types (Table 2), the cloud types that produce most of the total cloud effect on the in-atmosphere shortwave fluxes are cirrostratus, cirrus, and stratocumulus, with the former two cloud types decreasing the shortwave heating and the last one increasing the shortwave heating.

With a uniform mix of cloud types (Table 1), the three cloud types that produce most of the total cloud effect on the in-atmosphere longwave fluxes are (in descending order) deep convective, cirrostratus, and stratocumulus, with the former two cloud types decreasing the longwave cooling and the last one increasing the longwave cooling. With a realistic mix of cloud types (Table 2), the cloud types that produce most of the total cloud effect on the in-atmosphere longwave fluxes are stratocumulus, cumulus, and cirrus, with the former two cloud types increasing the longwave cooling and the last one decreasing the longwave cooling.

The overcast calculations highlight the effects of the changing relationship between clouds and water vapor when cloud height and optical thickness change. Changing cloud height and optical thickness changes the fraction of the sunlight that passes twice through the water vapor (and ozone) above the cloud, that is absorbed in the cloud layer, and that is absorbed by water vapor below the cloud. Since we did not consider a true ice phase model, treating all clouds as liquid, we have not shown the complete range of such changes with cloud type. Changing cloud height and optical thickness also changes the fraction of longwave radiation that is emitted from the water vapor (and $CO_2$) above the cloud, that is emitted by the cloud, and that is transmitted from the surface and water vapor below the cloud. Here, our treatment is most uncertain concerning the location of cloud base and its effect on the surface longwave fluxes. The climatology of cloud layer thicknesses used here (Zhang et al. 1995) exhibits a systematic increase of cloud layer thickness with increasing cloud-top heights that implies that cloud base heights do not increase as rapidly as cloud-top heights; however, since we have ignored the possibility of multiple cloud layers (see Chen et al. 1999, manuscript submitted to *J. Climate*),

we have probably still overestimated the cloud base height increases. Nevertheless, the fact that the shortwave and longwave, TOA and surface fluxes; and the cloud flux changes are not the same when the cloud properties are averaged spatially or both spatially and temporally before the calculation, even when the averaging procedure is linear in the radiative fluxes (see appendix), demonstrates that the correlations of cloud property variations with variations in water vapor and the surface alter the results. Although the global mean magnitude of the errors in the TOA and surface fluxes produced by such preaveraging is smaller on average than other sources of error (Zhang et al. 1995), so that it can be argued that such methods are justified, in fact these errors produce systematic shifts in the seasonal, latitudinal, and land–ocean contrasts in the radiation budget that are important for driving the atmospheric and oceanic circulations.

The magnitude of the flux errors produced by preaveraging the cloud properties is certainly significant when compared with the radiation budget changes that appear interannually or that are being considered in relation to possible climate changes induced by changes in atmospheric composition (increasing abundances of greenhouse gases and aerosols). This means that when considering possible cloud feedbacks on climate change, accurately capturing the changes in fluxes that might arise from changes in either the mean cloud properties or shifts in the relative abundance of different cloud types requires a separate treatment of their effects on the radiative fluxes as done here to capture the proper space–time correlations. Although we found, as did Hartmann and colleagues, that the cloud–radiative effects are dominated by a few cloud types, which cloud type is most important changes when considering different parts of the radiation budget. Thus, the complexity of the calculation cannot be reduced to fewer cloud types without reducing the accuracy of representing the correlations of the clouds and other atmospheric and surface properties in this climate problem. Moreover, such reduction cannot capture the full (nonlinear) effects of cloud property variations, including the varying relation between the shortwave and longwave effects (see Stubenrauch et al. 1999b). For example, even if the total cloud cover and *average* cloud properties remain fixed, a shift in the *distribution* of cloud types can change the radiation budget. This conclusion is strengthened by the fact that the cloud properties are strongly related to meteorological conditions (cf. Machado and Rossow 1993; Lau and Crane 1995); hence, the average radiative fluxes cannot be obtained without accounting for the varying correlations of clouds and atmospheric conditions with time and location (see also the appendix). Moreover, different cloud types may be associated with systematically different vertical structures (including layer structure, phase, and particle size changes, all unaccounted for in these calculations). Although less intensive calculations may be sufficiently accurate at the present time in representing the mean radiative fluxes, especially at TOA and at the surface, a much more detailed treatment is needed to capture the small *but systematic* effects of the correlations with meteorology, latitude, land–ocean conditions, and season that determine subtle radiative feedbacks that can be caused by changing cloud types.

Further work is required to include three effects not treated here. First, although there is uncertainty in locating cloud bases (Zhang et al. 1995), the most important deficiency is that we have not considered multiple cloud layers. Relative to our single-layered treatment, including multiple cloud layers would lower cloud bases on average, enhancing the effects of clouds on the surface longwave fluxes. This effect would be most important for any cloud type that has systematically larger layer thicknesses than assumed here, such as the deep convective clouds, or for any cloud type that frequently occurs with another lower-level cloud (cf. Warren et al. 1985), another form of correlation that must be accounted for. Second, in our treatment the cloud microphysical properties are fixed. The most notable systematic change that occurs is the change from liquid to ice going from warmer to colder temperatures, which would introduce both latitudinal and vertical variations in the cloud-radiative effects. However, there are also meteorological, seasonal, and regional variations in the clouds particle sizes (Han et al. 1994, 1998) that will also alter the cloud-radiative effects. Finally, to calculate nighttime radiative fluxes, we have had to interpolate the daytime results from ISCCP because the more accurate two-wavelength retrieval is only available then (see Stubenrauch et al. 1999a,b). Without better information about diurnal variations of cloud properties, the diagnosis of cloud-radiative effects is missing what could be another important correlation (e.g., see discussion in Machado and Rossow 1993).

*Acknowledgments.* We benefited from conversations with J. Key, B. A. Wielicki, P. Stackhouse, and G. L. Stephens. Douglas L. Cordero provided the 5-yr (1989–93) climatology of global mean cloud type amount from ISCCP D-series data. This work is supported by the NASA Radiation and Climate Program managed by Dr. Robert Curran and NSF Grant 9629237.

## APPENDIX

### Accuracy of Radiative Fluxes Determined from Average Cloud Properties

This appendix compares the aggregate radiative fluxes obtained from all the cloud types with those calculated using radiatively weighted averages of the cloud properties as done by Zhang et al. (1995) and others, and it also tests the accuracy of calculating the time-averaged cloud-induced radiative flux changes from preaveraged cloud, atmospheric, and surface properties

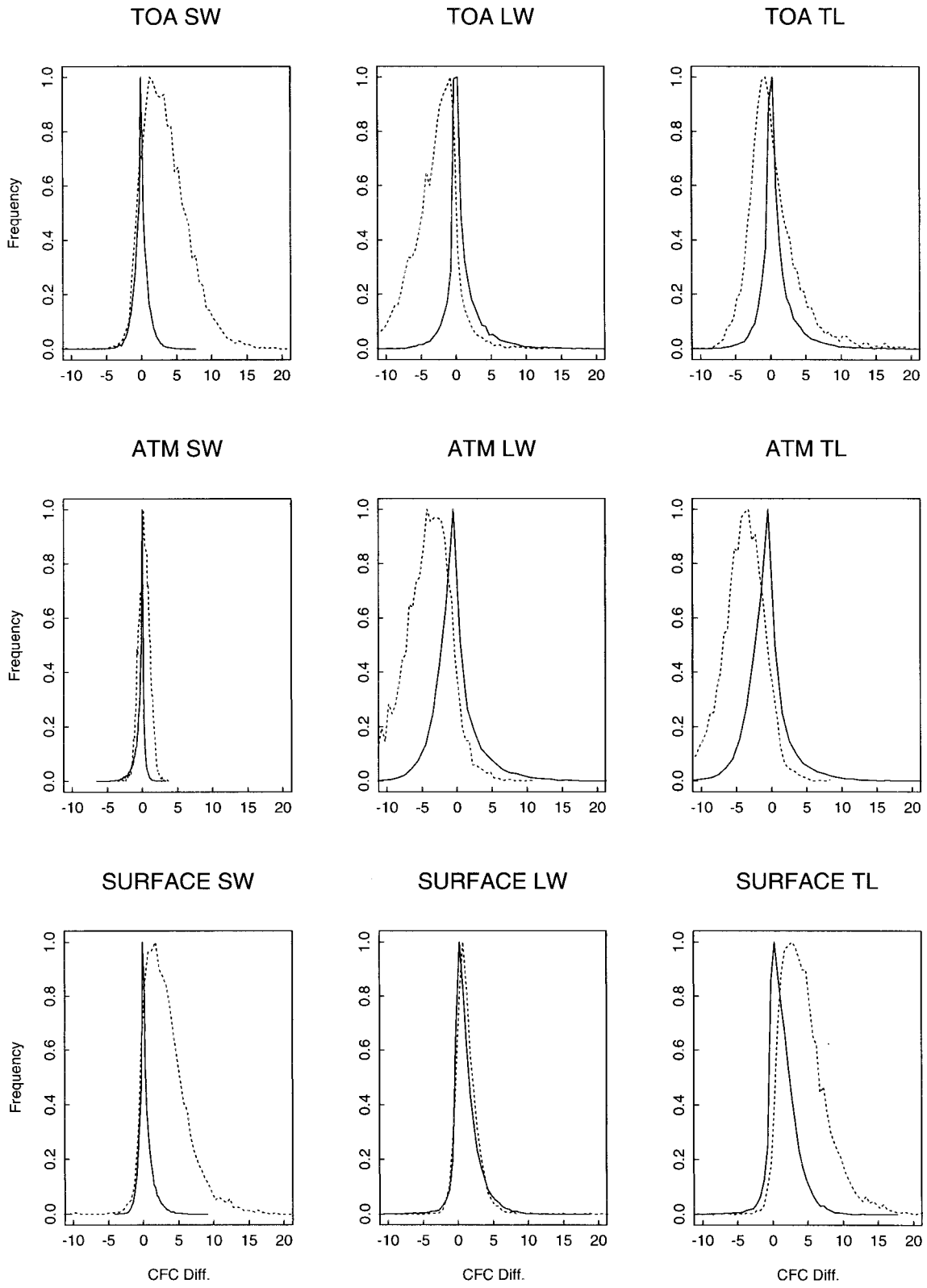


FIG. A1. Frequency histogram of the CFC differences average − true (solid line), monthly average − monthly true (dashed line); W $m^{-2}$).

TABLE A1. Global mean full sky cloud-induced radiative flux changes in W m$^{-2}$ at the surface, at TOA, and in-atmosphere from average, monthly average, and monthly true methods, together with the mean and the standard deviations (in parentheses) of the differences average − true and monthly average − monthly true.

| CFC | Surface | | | TOA | | | Atmosphere | | |
|---|---|---|---|---|---|---|---|---|---|
| | SW | LW | TL | SW | LW | TL | SW | LW | TL |
| Average | −52.3 | 25.5 | −26.8 | −53.5 | 20.9 | −32.6 | −1.2 | −4.6 | −5.8 |
| Average − True | 0.3 | 1.1 | 1.4 | 0.0 | 0.8 | 0.8 | −0.3 | −0.3 | −0.6 |
| (Std) | (1.0) | (1.9) | (2.0) | (1.0) | (2.6) | (2.5) | (0.7) | (3.2) | (3.0) |
| Monthly average | −41.7 | 25.3 | −16.4 | −43.0 | 18.7 | −24.3 | −1.3 | −6.6 | −7.9 |
| Monthly true | −45.0 | 24.0 | −21.0 | −46.5 | 21.8 | −24.7 | −1.5 | −2.2 | −3.7 |
| Monthly average − Monthly true | 3.3 | 1.3 | 4.6 | 3.5 | −3.1 | 0.4 | 0.2 | −4.4 | −4.2 |
| (Std dev) | (3.1) | (2.0) | (3.4) | (3.3) | (3.2) | (3.7) | (0.8) | (3.7) | (3.2) |

over time as done by Schweiger and Key (1994) for example.

In all of the calculations presented in the main text, the TOA and surface fluxes are calculated for clear sky and separately for each cloud type (overcast) at each place and time and then added in proportion to the amount of each cloud type and the amount of clear sky to obtain the full sky fluxes at each place and time. The corresponding daily mean fluxes and CFC values (called true) are computationally expensive (relatively) to ob-

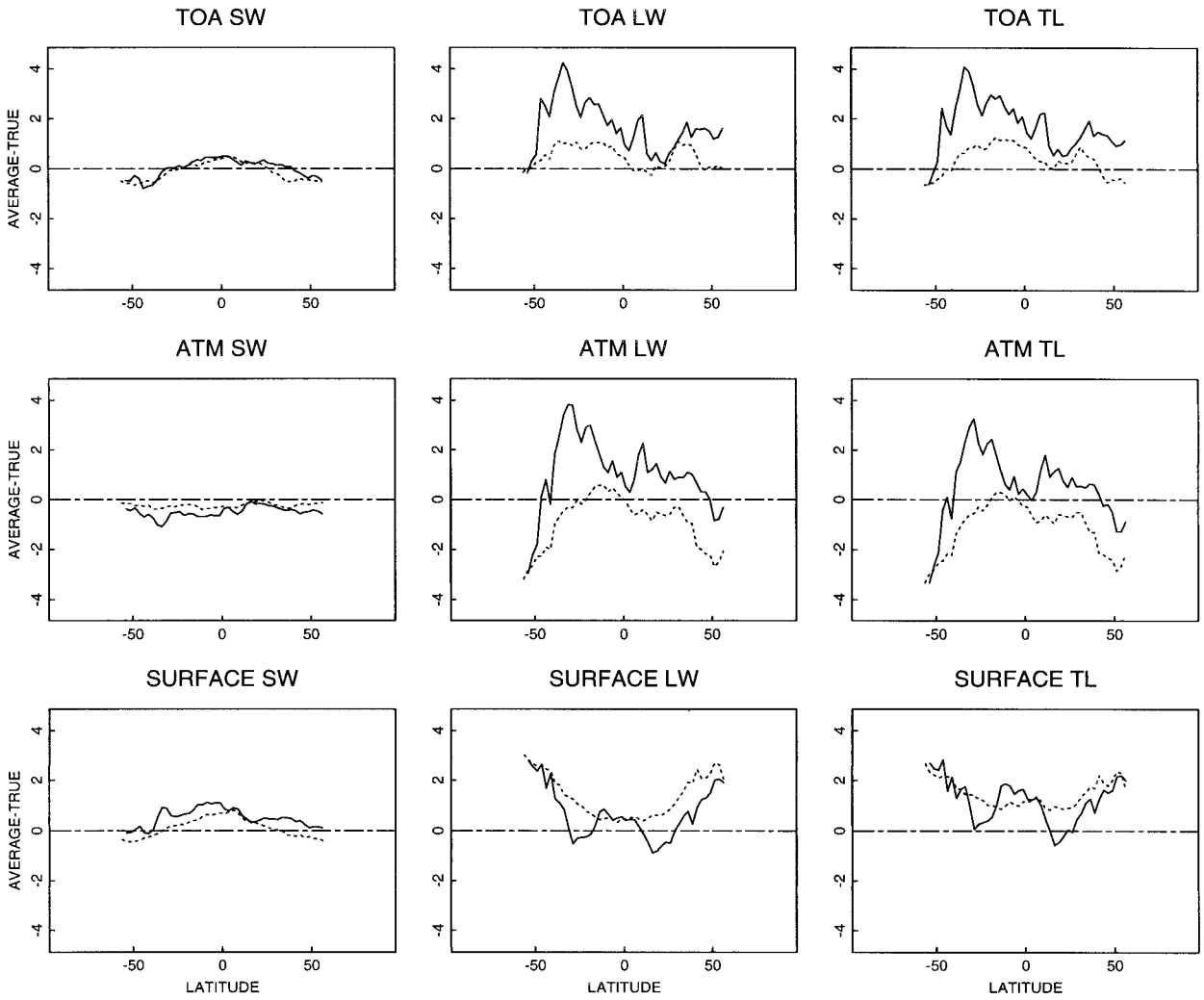


FIG. A2. Zonal mean distribution of the differences between the average and true CFC values (W m$^{-2}$) over land (solid line) and over ocean (dashed line).

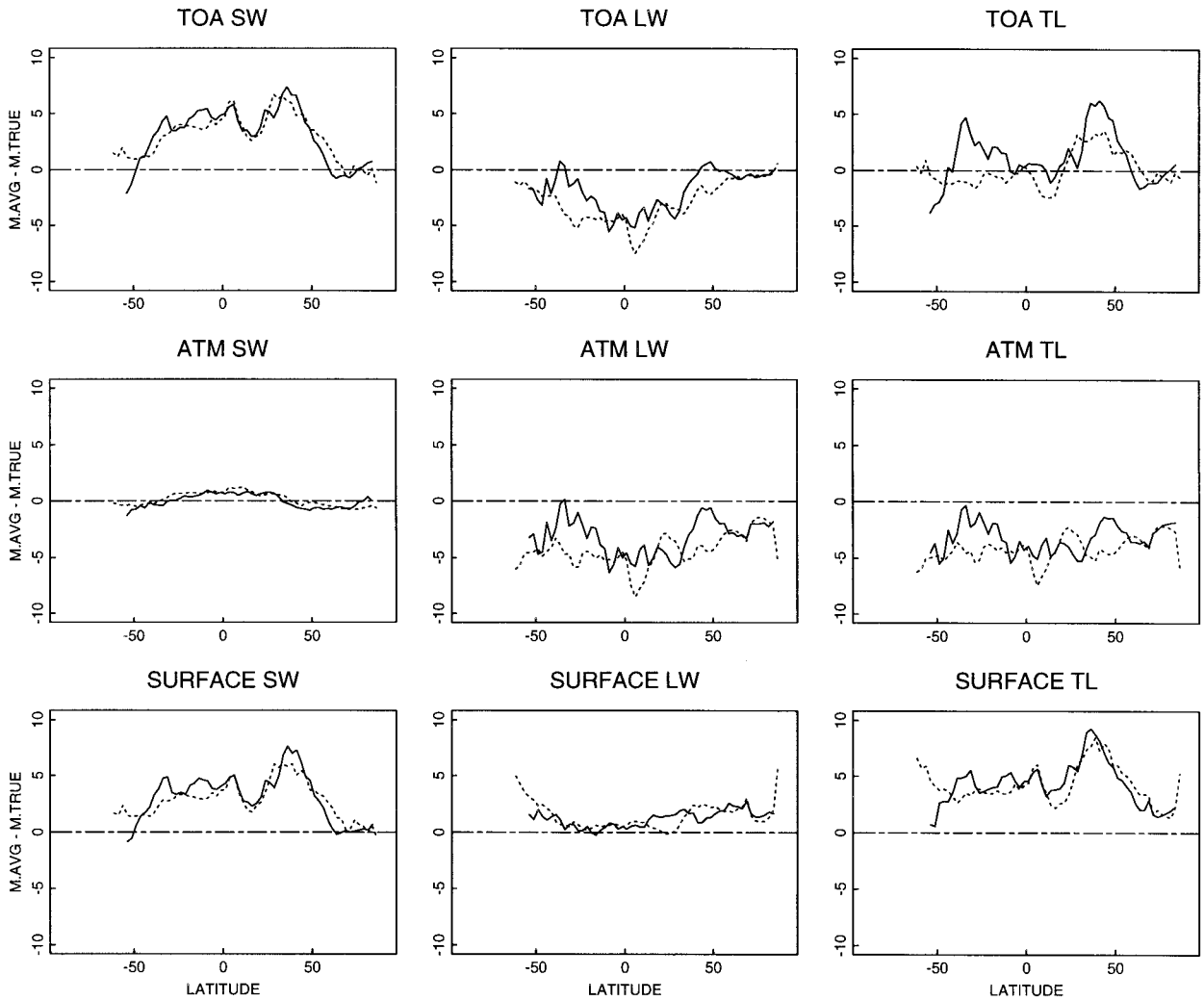


FIG. A3. Zonal mean distribution of the differences between the monthly average and monthly true CFC values (W $m^{-2}$) over land (solid line) and over ocean (dashed line).

tain. Rossow and Lacis (1990) and Zhang et al. (1995) saved computer time by first averaging the cloud properties within each map grid box at each time and then calculating the fluxes only for clear sky and for one (average) cloud; the full sky fluxes and CFC values are then determined by adding together these two results in proportion to the total cloud amount (called average) at each place and time. Schweiger and Key (1994), for example, save even more computer time by further averaging the cloud properties over time (e.g., a month) before calculating the fluxes (called monthly average; note that the cloud properties are radiatively averaged in this calculation) instead of averaging the calculated fluxes over time (called monthly true). We compare results from these different ways of performing the calculations to evaluate the importance of the interactions of the cloud-type properties with the spatial and temporal variations of the surface and atmosphere.

Table A1 gives the ''annual,'' global mean values of the shortwave, longwave, and total CFC values at the surface, at TOA, and in-atmosphere for average clouds (compare to true values in Table 2), together with the differences average − true. The solid lines in Fig. A1 shows the histogram of the regional differences of average − true. The global mean difference between average and true CFC values range from 0 to 0.3 W $m^{-2}$ (standard deviation $\leq$ 1.0 W $m^{-2}$) for the TOA and surface shortwave CFC and from 0.8 to 1.1 W $m^{-2}$ (standard deviation $\leq$ 2.6 W $m^{-2}$) for the TOA and surface longwave CFC. The in-atmosphere CFC differences have similar magnitudes. On average the fast two calculation methods agree well in estimating the TOA and surface CFC, but not the in-atmosphere CFC, since the magnitude of the in-atmosphere CFC differences is comparable with the in-atmosphere CFC values themselves. Regional TOA and surface CFC difference magnitudes can be as large as 5–10 W $m^{-2}$ (Fig. A1) and are positive slightly more often than they are negative.

Note that since the shortwave CFC values are generally negative, a positive difference between average and true means that the average calculation method underestimates the magnitude of the shortwave CFC; on the other hand, since the longwave CFC values are generally positive, a positive difference means that the average method overestimates the magnitude of the longwave CFC.

Table A1 also shows the global mean values of the various CFC components for the monthly average and monthly true methods using data from April 1991, together with the differences monthly average − monthly true. The dashed lines in Fig. A1 shows the histogram of the regional differences of monthly average − monthly true. The global mean difference between monthly average and monthly true CFC values range from 3.3 to 3.5 W $m^{-2}$ (standard deviation $\leq$3.3 W $m^{-2}$) for the surface and TOA shortwave CFC and from −3.1 to 1.3 W $m^{-2}$ (standard deviation $\leq$3.2 W $m^{-2}$) for the TOA and surface longwave CFC. The in-atmosphere CFC differences have similar magnitudes. Again these two calculation methods agree relatively well in estimating the TOA and surface CFC (but not the in-atmosphere CFC), although the differences between monthly average and monthly true CFC values are larger than the differences between average and true CFC values. Regional TOA and surface CFC difference magnitudes can be as large as 10–20 W $m^{-2}$ (Fig. A1) indicating the monthly average method does not capture the correlations of cloud property variations with variations in atmospheric and surface conditions as well.

Figures A2 and A3 illustrate the zonal mean distribution of the differences between the average and true (solid line) and the monthly average and monthly true CFC values (dashed line), showing that, though small in magnitude, the differences exhibit systematic patterns, including considerable differences over land relative to ocean. Such systematic differences would be important for determining the forcing of the atmospheric and oceanic circulations, and are likely to be significant compared with interannual anomalies.

## REFERENCES


Ackerman, T. P., K. N. Liou, F. P. J. Valero, and L. Pfister, 1988: Heating rates in tropical anvils. *J. Atmos. Sci.,* **45,** 1606–1623.

Charlson, R. J., J. Langner, H. Rodhe, C. B. Leovy, and S. G. Warren, 1991: Perturbation of the Northern Hemisphere radiative balance by backscattering from anthropogenic sulfate aerosols. *Tellus,* **43AB,** 152–163.

Curry, J. A., W. B. Rossow, D. Randall, and J. L. Schramm, 1996: Overview of Arctic cloud and radiation characteristics. *J. Climate,* **9,** 1731–1764.

Fung, I. Y., D. E. Harrison, and A. A. Lacis, 1984: On the variability of the net longwave radiation at the ocean surface. *Rev. Geophys. Space Phys.,* **22,** 177–193.

Han, Q., W. B. Rossow, and A. A. Lacis, 1994: Near-global survey of effective droplet radii in liquid water clouds using ISCCP data. *J. Climate,* **7,** 465–497.

——, ——, J. Chou, and R. M. Welch, 1998: Global survey of the relationships of cloud albedo and liquid water path with droplet size using ISCCP. *J. Climate,* **11,** 1516–1528.

Harrison, E. F., P. Minnis, B. R. Barkstrom, V. Ramanathan, R. D. Cess, and G. G. Gibson, 1990: Seasonal variation of cloud radiative forcing derived from the Earth Radiation Budget Experiment. *J. Geophys. Res.,* **95,** 18 687–18 703.

Hartmann, D. L., and D. Doelling, 1991: On the net radiative effectiveness of clouds. *J. Geophys. Res.,* **96,** 1204–1253.

——, V. Ramanathan, A. Berrior, and G. E. Hunt, 1986: Earth radiation budget data and climate research. *Rev. Geophys. Space Phys.,* **24,** 439–468.

——, M. E. Ockert-Bell, and M. L. Michelsen, 1992: The effect of cloud type on Earth's energy balance: Global analysis. *J. Climate,* **5,** 1281–1304.

Jin, Y., W. B. Rossow, and D. P. Wylie, 1996: Comparison of the climatologies of high-level clouds from HIRS and ISCCP. *J. Climate,* **9,** 2850–2854.

Kidwell, K. B., 1995: NOAA Polar Orbiter Data Users Guide (TIROS-N, NOAA-6, NOAA-7, NOAA-8, NOAA-9, NOAA-10, NOAA-11, NOAA-12, NOAA-13 and NOAA-14). National Environmental Satellite, Data and Information Service, Washington, DC, 394 pp.

Lau, N.-C., and M. W. Crane, 1995: A satellite view of the synoptic-scale organization of cloud properties in midlatitude and tropical circulation systems. *Mon. Wea. Rev.,* **123,** 1984–2006.

Liao, X., W. B. Rossow, and D. Rind, 1995: Comparison between SAGE II and ISCCP high-level clouds: Part 1: Global and zonal mean cloud amounts. *J. Geophys. Res.,* **100,** 1121–1135.

London, J., R. D. Bojkov, S. Oltmans, and J. I. Kelly, 1976: Atlas of the global distribution of total ozone, July 1957–June 1967. NCAR Tech. Note 113 + STR, National Center for Atmospheric Research, Boulder, CO, 276 pp.

Machado, L. A. T., and W. B. Rossow, 1993: Structural characteristics and radiative properties of tropical cloud clusters. *Mon. Wea. Rev.,* **121,** 3234–3260.

Matthews, E., 1983: Global vegetation and land-use: New high-resolution data bases for climate studies. *J. Climate Appl. Meteor.,* **22,** 474–487.

——, 1984: Prescription of land-surface boundary conditions in GISS GCM II: A simple method based on fine-resolution data bases. NASA Tech. Memo. 86096, 20 pp.

Minnis, P., P. W. Heck, and D. F. Young, 1993: Inference of cirrus cloud properties using satellite-observed visible and infrared radiances. Part II: Verification of theoretical cirrus radiative properties. *J. Atmos. Sci.,* **50,** 1305–1322.

Mishchenko, M. I., W. B. Rossow, A. Macke, and A. A. Lacis, 1996: Sensitivity of cirrus cloud albedo, bidirectional reflectance and optical thickness retrieval accuracy to ice particle shape. *J. Geophys. Res.,* **101,** 16 973–16 985.

Ockert-Bell, M. E., and D. L. Hartmann, 1992: The effect of cloud type on earth's energy balance: Results for selected regions. *J. Climate,* **5,** 1158–1171.

Oort, A. H., 1983: Global Atmospheric Circulation Statistics, 1958–1973. NOAA Professional Paper 14, NOAA Geophysical Fluid Dynamics Laboratory, 180 pp.

Poore, K., J. Wang, and W. B. Rossow, 1995: Cloud layer thicknesses from a combination of surface and upper air observations. *J. Climate,* **8,** 550–568.

Rossow, W. B., and A. A. Lacis, 1990: Global, seasonal cloud variations from satellite radiance measurements. Part II: Cloud properties and radiative effects. *J. Climate,* **3,** 1204–1253.

——, and R. A. Schiffer, 1991: ISCCP cloud data products. *Bull. Amer. Meteor. Soc.,* **72,** 2–20.

——, and Y.-C. Zhang, 1995: Calculation of surface and top of atmosphere radiative fluxes from physical quantities based on ISCCP data sets. Part 2: Validation and first results. *J. Geophys. Res.,* **100,** 1167–1197.

——, A. W. Walker, D. E. Beuschel, and M. D. Roiter, 1996: International Satellite Cloud Climatology Project (ISCCP) Documentation of New Cloud Datasets. Tech. Doc. WMO/TD 737, World Climate Research Programme, Geneva, Switzerland, 115 pp.

Schiffer, R. A., and W. B. Rossow, 1983: The International Satellite Cloud Climatology Project (ISCCP): The first project of the World Climate Research Programme. *Bull. Amer. Meteor. Soc.*, **64,** 779–784.

——, and ——, 1985: ISCCP global radiance data set: A new resource for climate research. *Bull. Amer. Meteor. Soc.*, **66,** 1498–1505.

Schweiger, A. J., and J. R. Key, 1994: Arctic Ocean radiative fluxes and cloud forcing estimated from the ISCCP C2 cloud dataset, 1983–1990. *J. Appl. Meteor.*, **33,** 948–963.

Stubenrauch, C. J., W. B. Rossow, F. Cheruy, A. Chedin, and N. A. Scott, 1999a: Clouds as seen by satellite sounders (3I) and imagers (ISCCP). Part I: Evaluation of cloud parameters. *J. Climate,* **12,** 2189–2213.

——, ——, N. A. Scott, and A. Chedin, 1999b: Clouds as seen by satellite sounders (3I) and imagers (ISCCP). Part III: Spatial heterogeneity and radiative effects. *J. Climate,* **12,** 3419–3442.

Toon, O. B., and J. B. Pollack, 1976: A global average model of atmospheric aerosols for radiative transfer calculations. *J. Appl. Meteor.*, **15,** 225–246.

Wang, J., and W. B. Rossow, 1995: Determination of cloud vertical structure from upper-air observations. *J. Appl. Meteor.*, **34,** 2243–2258.

Warren, S. G., C. J. Hahn, and J. London, 1985: Simultaneous occurrence of different cloud types. *J. Climate Appl. Meteor.*, **24,** 658–667.

——, ——, R. M. Chervin, and R. L. Jenne, 1986: Global distribution of total cloud cover and cloud type amounts over land. NCAR Tech. Note NCAR/TN-273+STR, National Center for Atmospheric Research, Boulder, CO, 29 pp.+ 200 maps.

——, ——, J. London, R. M. Chervin, and R. L. Jenne, 1988: Global distribution of total cloud cover and cloud type amounts over ocean. NCAR Tech. Note NCAR/TN-317+STR, National Center for Atmospheric Research, Boulder, CO, 42 pp. + 170 maps.

Webster, P. J., and G. L. Stephens, 1984: Cloud–radiation interaction and the climate problems. *The Global Climate*, J. T. Houghton, Ed., Cambridge University Press, 63–78.

Zhang, Y.-C., and W. B. Rossow, 1997: Estimating meridional energy transports by the atmospheric and oceanic general circulations using boundary flux data. *J. Climate,* **10,** 2358–2373.

——, ——, and A. A. Lacis, 1995: Calculation of surface and top of atmosphere radiative fluxes from physical quantities based on ISCCP data sets. Part 1: Method and sensitivity to input data uncertainties. *J. Geophys. Res.,* **100,** 1149–1165.